

2

NATIONAL AERONAUTICS AND SPACE ADMINISTRATION

*Technical Memorandum 33-624*

*Analysis and Simulation of the Mariner Mars  
1971 Scan Platform: Spacecraft Dynamic  
Interaction*

*L. Schumacher*

(NASA-CR-133793) ANALYSIS AND SIMULATION  
OF THE MARINER MARS 1971 SCAN PLATFORM:  
SPACECRAFT DYNAMIC INTERACTION (Jet  
Propulsion Lab.) 62 p HC \$5.25 CSCL 22B  
65

N73-30837

G3/31 Unclass  
13123

Reproduced by  
NATIONAL TECHNICAL  
INFORMATION SERVICE  
US Department of Commerce  
Springfield, VA. 22151

JET PROPULSION LABORATORY  
CALIFORNIA INSTITUTE OF TECHNOLOGY  
PASADENA, CALIFORNIA

August 15, 1973

65

TECHNICAL REPORT STANDARD TITLE PAGE

1. Report No. 33-624		2. Government Accession No.		3. Recipient's Catalog No.	
4. Title and Subtitle ANALYSIS AND SIMULATION OF THE MARINER MARS 1971 SCAN PLATFORM: SPACECRAFT DYNAMIC INTERACTION				5. Report Date August 15, 1973	
				6. Performing Organization Code	
7. Author(s) L. Schumacher				8. Performing Organization Report No.	
9. Performing Organization Name and Address JET PROPULSION LABORATORY California Institute of Technology 4800 Oak Grove Drive Pasadena, California 91103				10. Work Unit No.	
				11. Contract or Grant No. NAS 7-100	
12. Sponsoring Agency Name and Address NATIONAL AERONAUTICS AND SPACE ADMINISTRATION Washington, D.C. 20546				13. Type of Report and Period Covered Technical Memorandum	
				14. Sponsoring Agency Code	
15. Supplementary Notes					
16. Abstract  The Mariner spacecraft as well as most other spacecraft have instrument platforms, antennas, etc., which must move relative to the attitude controlled spacecraft bus structure. As the appendages are moved, reaction forces and torques are produced that disturb the spacecraft attitude. This report develops the equations of motion which describe the dynamic interaction between the spacecraft bus and the movable appendages about a single axis, evaluates the effect of the dynamic interaction on the attitude control subsystem with computer simulations, and makes design recommendations to reduce the impact of this interaction on future attitude control subsystems.					
17. Key Words (Selected by Author(s)) Control and Guidance Mariner Mars 1971 Project Telemetry and Command Spacecraft Modeling			18. Distribution Statement Unclassified -- Unlimited		
19. Security Classif. (of this report) Unclassified	20. Security Classif. (of this page) Unclassified		21. No. of Pages 55	22. Price	

## HOW TO FILL OUT THE TECHNICAL REPORT STANDARD TITLE PAGE

Make items 1, 4, 5, 9, 12, and 13 agree with the corresponding information on the report cover. Use all capital letters for title (item 4). Leave items 2, 6, and 14 blank. Complete the remaining items as follows:

3. Recipient's Catalog No. Reserved for use by report recipients.
7. Author(s). Include corresponding information from the report cover. In addition, list the affiliation of an author if it differs from that of the performing organization.
8. Performing Organization Report No. Insert if performing organization wishes to assign this number.
10. Work Unit No. Use the agency-wide code (for example, 923-50-10-06-72), which uniquely identifies the work unit under which the work was authorized. Non-NASA performing organizations will leave this blank.
11. Insert the number of the contract or grant under which the report was prepared.
15. Supplementary Notes. Enter information not included elsewhere but useful, such as: Prepared in cooperation with... Translation of (or by)... Presented at conference of... To be published in...
16. Abstract. Include a brief (not to exceed 200 words) factual summary of the most significant information contained in the report. If possible, the abstract of a classified report should be unclassified. If the report contains a significant bibliography or literature survey, mention it here.
17. Key Words. Insert terms or short phrases selected by the author that identify the principal subjects covered in the report, and that are sufficiently specific and precise to be used for cataloging.
18. Distribution Statement. Enter one of the authorized statements used to denote releasability to the public or a limitation on dissemination for reasons other than security of defense information. Authorized statements are "Unclassified-Unlimited," "U. S. Government and Contractors only," "U. S. Government Agencies only," and "NASA and NASA Contractors only."
19. Security Classification (of report). NOTE: Reports carrying a security classification will require additional markings giving security and downgrading information as specified by the Security Requirements Checklist and the DoD Industrial Security Manual (DoD 5220.22-M).
20. Security Classification (of this page). NOTE: Because this page may be used in preparing announcements, bibliographies, and data banks, it should be unclassified if possible. If a classification is required, indicate separately the classification of the title and the abstract by following these items with either "(U)" for unclassified, or "(C)" or "(S)" as applicable for classified items.
21. No. of Pages. Insert the number of pages.
22. Price. Insert the price set by the Clearinghouse for Federal Scientific and Technical Information or the Government Printing Office, if known.

NATIONAL AERONAUTICS AND SPACE ADMINISTRATION

*Technical Memorandum 33-624*

*Analysis and Simulation of the Mariner Mars  
1971 Scan Platform: Spacecraft Dynamic  
Interaction*

*L. Schumacher*

JET PROPULSION LABORATORY  
CALIFORNIA INSTITUTE OF TECHNOLOGY  
PASADENA, CALIFORNIA

August 15, 1973

Prepared Under Contract No. NAS 7-100  
National Aeronautics and Space Administration

PRECEDING PAGE BLANK NOT FOLLOWS

## PREFACE

The work described in this report was performed by the Guidance and Control Division of the Jet Propulsion Laboratory.

# CONTENTS

I.	Introduction. . . . .	1
II.	Analysis of the Dynamic Interaction Between Two Bodies Moving Relative to Each Other About a Single Axis. . . . .	2
	A. Equations of Motion About the Axis of Revolution. . . . .	2
	B. Equations of Motion About Axes Orthogonal to the Scan Platform Axis of Revolution . . . . .	6
	1. Single-degree-of-freedom platform. . . . .	6
	2. Two-degree-of-freedom scan platform. . . . .	7
III.	Computer Simulations of MM'71 Scan Platform Dynamic Interaction . . . . .	11
	A. Scan Platform Dynamic Model Development . . . . .	12
	B. Scan Platform Dynamic Interaction Computer Simulation Results . . . . .	14
IV.	Analytical Evaluation of MM'71 Scan Platform Dynamic Interaction . . . . .	17
	A. Cone-Axis Scan Platform Slewing Configuration and Disturbances . . . . .	17
	1. Axis of revolution configuration and disturbances (cone slew) . . . . .	17
	2. Configuration and disturbances in the axis orthogonal to the cone slewing axis . . . . .	18
	B. Clock-Axis Scan Platform Slewing Configuration and Disturbances . . . . .	18
	1. Axis of revolution configuration and disturbances (clock slew) . . . . .	18
	2. Configuration and disturbances in the axis orthogonal to the clock slewing axis. . . . .	19
V.	Attitude Control Gas Consumption Resulting from the Forced Relative Motion of Two Bodies in Space. . . . .	20
	A. Determination of the Angular Momentum in Each of the Three Spacecraft Axes as a Result of the Forced Relative Motion of Two Bodies . . . . .	20

## CONTENTS (contd)

B.	Determination of the Gas Required to Remove the Angular Momentum Resulting From the Forced Relative Motion of Two Bodies . . . . .	21
C.	Summary and Conclusions . . . . .	25
VI.	Design and Control of Articulated Spacecraft Platforms . . . . .	26
A.	Design Objective	
B.	Design and Location of Articulated Spacecraft Packages . . . . .	27
C.	Articulated Package Actuator and Control Design Guidelines. . . . .	28
D.	Guideline Summary. . . . .	28
VII.	Conclusion . . . . .	29
Appendix A.	Scan Design Analysis . . . . .	47
Appendix B.	Scan Design Analysis Modification. . . . .	49
Appendix C.	Determination of Relative Scan Platform Rate and Position Expressions . . . . .	50
Nomenclature	. . . . .	53
References	. . . . .	55

## TABLES

1.	MM'71 scan-axis parameter evaluation . . . . .	30
2.	MM'71 slewing gas consumption parameter definitions . . . . .	31

## FIGURES

1.	MM'71 cone-axis configuration . . . . .	32
2.	Simplified spacecraft bus and platform configuration and free-body diagram . . . . .	33
3.	Spacecraft mass-centered coordinate system and scan hinge point. . . . .	34
4.	Spacecraft/platform model with reaction force from a scan slew. . . . .	34

## CONTENTS (contd)

### FIGURES (contd)

5.	Scan platform model development components: a. Logic sequence for scan stepper motor commands, b. Scan actuator displacement, c. Scan actuator model . . . . .	35
6.	Scan platform dynamic models: a. Scan control linear servo, b. Scan spring/mass/damper, c. Improved scan linear servo . . . . .	36
7.	Scan platform model angular displacements . . . . .	37
8.	Scan platform model angular rates . . . . .	38
9.	Roll-axis phase plane during a scan slew; rate disturbance exceeds roll-axis rate plus position deadband . . . . .	39
10.	Roll-axis phase plane during a scan slew; roll rate is less than total rate deadband . . . . .	40
11.	Comparison of actual and simulated spacecraft position values during a clock-axis slew: a. Pitch, b. Yaw, c. Roll . . . . .	41
12.	Spacecraft rate and position during two 0.25-deg cone-axis steps . . . . .	42
13.	MM'71 clock-axis configuration . . . . .	43
14.	Spacecraft rate and position during two 0.25-deg clock-axis steps . . . . .	44
15.	Center-of-mass relationships before and after a scan slew . . . . .	45
16.	Spacecraft phase plane during (a) long- and (b) short-duration slews . . . . .	46

## ABSTRACT

The Mariner spacecraft as well as most other spacecraft have instrument platforms, antennas, etc., which must move relative to the attitude controlled spacecraft bus structure. As the appendages are moved, reaction forces and torques are produced that disturb the spacecraft attitude. This report develops the equations of motion which describe the dynamic interaction between the spacecraft bus and the movable appendages about a single axis, evaluates the effect of the dynamic interaction on the attitude control subsystem with computer simulations, and makes design recommendations to reduce the impact of this interaction on future attitude control subsystems.

## I. INTRODUCTION

In terms of scan platform dynamics, the Mariner Mars 1971 (MM'71) spacecraft could be thought of as two bodies connected by an actuating mechanism. The principal body was the spacecraft bus structure containing the attitude control system celestial and inertial sensors. The second body was the scan platform, which contained all the science instruments, including the TV cameras.

As the scan platform was moved relative to the spacecraft bus, large forces and torques were observed in the spacecraft position sensor telemetry data. These disturbances had been predicted, but their magnitude was greater than expected.

The study presented here was undertaken in order to resolve the conflict between predicted and actual slewing disturbances, and to determine their effect on the attitude control gas consumption.

The scan platform/spacecraft bus dynamic interaction was investigated at two levels. The flight observed performance was reproduced almost exactly using a new and powerful computer program which solves the equations of motion of simply connected rigid bodies. This program enabled mission support analysts to better predict dynamic disturbances and gas consumption but did not explain the mechanism of these disturbances. In parallel with the computer simulation analysis, a single-axis analytic model was developed which not only predicted the dynamic disturbance magnitudes accurately but also revealed their mechanism.

This report describes the analysis methods, discusses the development of the MM'71 spacecraft scan platform model, and demonstrates the accuracy of the computer modeling technique by making comparisons to actual flight data. In addition, methods are presented to estimate attitude control gas consumption resulting from scan slews, and guidelines are established which will enable future articulation system designers to minimize the disturbances resulting from platform articulation in space.

## II. ANALYSIS OF THE DYNAMIC INTERACTION BETWEEN TWO BODIES MOVING RELATIVE TO EACH OTHER ABOUT A SINGLE AXIS

A complete description of the motion of two bodies in space moving relative to each other about an arbitrary single axis would require that equations be written for eight degrees of freedom. However, for the purposes of design and understanding, the motion of interest can be described using a single-axis development. For example, Fig. 1 illustrates the MM'71 bus structure and a two-degree-of-freedom scan platform, with the cone axis of revolution perpendicular to the plane of the paper and the clock axis in the plane of the paper. The single-axis equations of motion about the axis of rotation for both the cone and clock axes are the same. The forces produced at the hinge point in the plane perpendicular to the axis of revolution produce disturbance torques in the axes orthogonal to the slewing axis. The equations of motion describing both of these conditions are developed for a general two-body configuration,\* so that the analytical techniques will be applicable to any spacecraft configuration with the appropriate parameter substitutions. Examples of parameter determination and substitution will be given using the MM'71 scan platform configuration.

### A. Equations of Motion About the Axis of Revolution

A hypothetical spacecraft bus structure and scan platform configuration is illustrated in Fig. 2, with a free-body diagram of the bus and platform during a rotation of the platform about an axis perpendicular to the

---

\*The analytical formulation of this problem and many of the following expressions the result of the original work of G. E. Fleischer.

plane of the figure. The torque equations about the center of mass of the scan platform and spacecraft bus, respectively, are given by

$$I_{sn} \ddot{\theta}_{sn} = T_h - f_h(\dot{\theta}_{sn} - \dot{\theta}_{s/c}) - F_x k \sin \theta_{sn} + F_y k \cos \theta_{sn} \quad (1)$$

$$I_{s/c} \ddot{\theta}_{s/c} = -T_h + f_h(\dot{\theta}_{sn} - \dot{\theta}_{s/c}) + F_y \ell \cos \theta_{s/c} - F_x \ell \sin \theta_{s/c} \quad (2)$$

The force equations on the spacecraft bus and scan platform respectively are

$$\begin{aligned} F_x &= m_{s/c} \ddot{X}_{s/c} \\ F_y &= m_{s/c} \ddot{Y}_{s/c} \end{aligned} \quad (3)$$

$$\begin{aligned} F_x &= -m_{sn} \ddot{X}_{sn} \\ F_y &= -m_{sn} \ddot{Y}_{sn} \end{aligned} \quad (4)$$

From Fig. 1, it can be observed that

$$\begin{aligned} X_{sn} &= X_{s/c} + \ell \cos \theta_{s/c} + k \cos \theta_{sn} \\ Y_{sn} &= Y_{s/c} + \ell \sin \theta_{s/c} + k \sin \theta_{sn} \end{aligned} \quad (5)$$

Differentiating the equations above twice and substituting from Eqs. (3) and (4), we find

$$\begin{aligned} F_x &= \frac{m_{s/c} m_{sn}}{m_{s/c} + m_{sn}} \left( \ell \cos \theta_{s/c} \dot{\theta}_{s/c}^2 + \ell \sin \theta_{s/c} \ddot{\theta}_{s/c} \right. \\ &\quad \left. + k \cos \theta_{sn} \dot{\theta}_{sn}^2 + k \sin \theta_{sn} \ddot{\theta}_{sn} \right) \end{aligned} \quad (6)$$

$$F_y = \frac{m_{s/c} m_{sn}}{m_{s/c} + m_{sn}} \left( \ell \sin \theta_{s/c} \dot{\theta}_{s/c}^2 - \ell \cos \theta_{s/c} \ddot{\theta}_{s/c} + k \sin \theta_{sn} \dot{\theta}_{sn}^2 - k \cos \theta_{sn} \ddot{\theta}_{sn} \right) \quad (7)$$

Let

$$m = \frac{m_{s/c} m_{sn}}{m_{s/c} + m_{sn}} \quad (8)$$

and

$$T_h = k_h (\theta_{snc} + \theta_{s/c} - \theta_{sn}) \quad (9)$$

so that, substituting Eqs. (6) through (9) into (1) and (2), we find that

$$(I_{sn} + mk^2) \ddot{\theta}_{sn} + mkl \cos (\theta_{s/c} - \theta_{sn}) \ddot{\theta}_{s/c} - mkl \sin (\theta_{s/c} - \theta_{sn}) \dot{\theta}_{s/c}^2 + f_h (\dot{\theta}_{sn} - \dot{\theta}_{s/c}) + k_h (\theta_{sn} - \theta_{s/c} - \theta_{snc}) = 0 \quad (10)$$

and

$$(I_{s/c} + ml^2) \ddot{\theta}_{s/c} + mlk \cos (\theta_{s/c} - \theta_{sn}) \ddot{\theta}_{sn} + mlk \sin (\theta_{s/c} - \theta_{sn}) \dot{\theta}_{sn}^2 + f_h (\dot{\theta}_{s/c} - \dot{\theta}_{sn}) + k_h (\theta_{snc} + \theta_{s/c} - \theta_{sn}) = 0 \quad (11)$$

Equations (10) and (11) describe the rotational motion of the scan platform and spacecraft bus in inertial coordinates. In actual flight, however, only the inertial displacement of the spacecraft bus can be observed, while the relative displacement and rate between the scan platform and the bus structure are known functions of the scan actuator design and are determined

from preflight tests. The displacement of the scan platform relative to the spacecraft bus can be determined by

$$\theta_{sn} = \theta_{s/c} + \theta_q \quad (12)$$

Performing the required differentiation on Eq. (12) and substituting into Eqs. (10) and (11), we determine the following expression, which describes the motion of the spacecraft in terms of the known platform relative displacement, rate, and acceleration:

$$\begin{aligned} (I_{sn} + mk^2)\ddot{\theta}_q + [I_{sn} + mk^2 + mkl \cos(\theta_q)]\ddot{\theta}_{s/c} \\ + mkl \sin(\theta_q)\dot{\theta}_{s/c}^2 + f_h(\dot{\theta}_q) + k_h(\theta_q - \theta_{snc}) = 0 \end{aligned} \quad (13)$$

$$\begin{aligned} - [I_{s/c} + m\ell^2 + m\ell k \cos(\theta_q)]\ddot{\theta}_{s/c} + m\ell k \cos \theta_q \ddot{\theta}_q \\ - m\ell k \sin(\theta_q) \left( \dot{\theta}_{s/c}^2 + 2\dot{\theta}_{s/c}\dot{\theta}_q + \dot{\theta}_q^2 \right) - f_h(\dot{\theta}_q) + k_h(\theta_{snc} - \theta_q) = 0 \end{aligned} \quad (14)$$

Assuming that all rate products are small relative to other terms, we can solve Eqs. (13) and (14) for the ratio of the spacecraft bus inertial acceleration to platform relative acceleration as follows:

$$\frac{\ddot{\theta}_{s/c}}{\ddot{\theta}_q} = \frac{- \left\{ I_{sn} + m[k^2 + \ell k \cos(\theta_q)] \right\}}{I_{s/c} + I_{sn} + m[k^2 + \ell^2 + 2\ell k \cos(\theta_q)]} \quad (15)$$

When the initial spacecraft rate and scan slew rate are zero, the above ratio is also the ratio of the spacecraft rate to slew rate.

In Section III, it will be demonstrated that the above ratio is accurate to within 5% and can be used to determine the magnitude of the slewing

disturbance observed by the spacecraft bus about the axis of platform revolution.

B. Equations of Motion About Axes Orthogonal to the Scan Platform Axis of Revolution

1. Single-degree-of-freedom platform. The free-body diagram in Fig. 2 shows that reaction forces are produced at the axis of revolution or hinge point in a plane perpendicular to the axis of platform revolution.\* These forces may be resolved along the spacecraft coordinate axes, and the disturbance torques produced by them can be evaluated if the position of the spacecraft bus center of mass is known relative to the platform hinge point.

A hypothetical right-handed spacecraft bus mass-centered coordinate system is illustrated in Fig. 3, with reaction forces from a scan platform slew located at some hinge coordinates  $P_h$ ,  $Y_h$ ,  $R_h$ . The torque produced by these forces is expressed by

$$T_p = -F_y R_h + F_r Y_h \quad (16)$$

$$T_y = F_p R_h - F_r P_h \quad (17)$$

$$T_r = F_y P_h - F_p Y_h \quad (18)$$

If the spacecraft bus products of inertia are small relative to the moments of inertia, the products of all angular rates are small, and the platform has only one degree of freedom, we can make the following approximation:

$$T_p = I_{pp} \ddot{\theta}_p \quad (19)$$

$$T_y = I_{yy} \ddot{\theta}_y \quad (20)$$

$$T_r = I_{rr} \ddot{\theta}_r \quad (21)$$

---

\*This analysis assumes that the spacecraft bus, scan platform, and hinge axis are in the same plane.

If the angular rate products are also assumed small in the evaluation of  $F_x$  and  $F_y$  from Eqs. (6) and (7), we can make the approximation:

$$F_x = f(\theta_{sn})\ddot{\theta}_{sn} \quad (22)$$

$$F_y = g(\theta_{sn})\ddot{\theta}_{sn} \quad (23)$$

When  $F_x$  and  $F_y$  from Eqs. (22) and (23) are resolved into  $F_p$ ,  $F_y$ , and  $F_r$  in Eqs. (16), (17), and (18), the ratio of the spacecraft angular acceleration to scan slewing acceleration in each axis can be determined.

2. Two-degree-of-freedom scan platform. A hypothetical spacecraft and scan platform are illustrated in Fig. 4. The difference between Figs. 2 and 4 is that a force has been added to the spacecraft bus in Fig. 4, and there are no commanded changes in the relative position of the scan platform. The force is applied at the scan hinge point and is in the plane of the figure. This force is a reaction force on the spacecraft resulting from a slew about an axis orthogonal to the force and in the plane of the figure. In this section, we will derive the single-axis equations of motion of a spacecraft and scan platform about an axis orthogonal to the slewing axis. There are two assumptions made in this derivation which make it substantially different from the derivation of motion about the slewing axis:

- (1) The products of inertia terms containing angular accelerations contribute significantly to the evaluation of disturbances in axes orthogonal to the slewing axes.
- (2) For a large spacecraft, the torque produced by the reaction forces in the axes orthogonal to the slewing axes do not accelerate the spacecraft enough to cause large differences in the inertial scan acceleration ( $\ddot{\theta}_{sn}$ ) and the inertial spacecraft acceleration ( $\ddot{\theta}_{s/c}$ ). Therefore, in the axes orthogonal to the slewing axes,  $\ddot{\theta}_{s/c}$  will be assumed equal to  $\ddot{\theta}_{sn}$ , or

$$\ddot{\theta}_{s/c} = \ddot{\theta}_{sn} \quad (24)$$

The torque equations about the center of mass of the spacecraft bus and scan platform, respectively, are

$$I_{s/c} \ddot{\theta}_{s/c} = (F_y + F \sin \theta_f) \ell \cos \theta_{s/c} - (F_x + F \cos \theta_f) \ell \sin \theta_{s/c} + T_H + f_h (\dot{\theta}_{sn} - \dot{\theta}_{s/c}) + I_{sx} \ddot{\theta}_x + I_{sy} \ddot{\theta}_y \quad (25)$$

$$I_{sn} \ddot{\theta}_{sn} = F_y k \cos \theta_{sn} - F_x k \sin \theta_{sn} - T_H - f_h (\dot{\theta}_{sn} - \dot{\theta}_{s/c}) \quad (26)$$

The force equations on the spacecraft bus and scan platform, respectively, are given by

$$\begin{aligned} F_x + F \cos \theta_f &= m_{s/c} \ddot{X}_{s/c} \\ F_y + F \sin \theta_f &= m_{s/c} \ddot{Y}_{s/c} \end{aligned} \quad (27)$$

$$\begin{aligned} F_x &= -m_{sn} \ddot{X}_{sn} \\ F_y &= -m_{sn} \ddot{Y}_{sn} \end{aligned} \quad (28)$$

From Fig. 4, it can be observed that

$$\begin{aligned} X_{sn} &= X_{s/c} + \ell \cos \theta_{s/c} + k \cos \theta_{sn} \\ Y_{sn} &= Y_{s/c} + \ell \sin \theta_{s/c} + k \sin \theta_{sn} \end{aligned} \quad (29)$$

Differentiating the above equations twice and substituting from Eqs. (27) and (28), we find that

$$\begin{aligned} F_x = - \frac{m_{s/c} m_{sn}}{m_{s/c} + m_{sn}} & \left( \frac{F \cos \theta_f}{m_{s/c}} - \ell \cos \theta_{s/c} \dot{\theta}_{s/c}^2 \right. \\ & \left. - \ell \sin \theta_{s/c} \ddot{\theta}_{s/c} - k \cos \theta_{sn} \dot{\theta}_{sn}^2 - k \sin \theta_{sn} \ddot{\theta}_{sn} \right) \end{aligned} \quad (30)$$

$$F_y = - \frac{m_{s/c} m_{sn}}{m_{s/c} + m_{sn}} \left( \frac{F \sin \theta_f}{m_{s/c}} - \ell \sin \theta_{s/c} \dot{\theta}_{s/c}^2 + \ell \cos \theta_{s/c} \ddot{\theta}_{s/c} - k \sin \theta_{sn} \dot{\theta}_{sn}^2 + k \cos \theta_{sn} \ddot{\theta}_{sn} \right) \quad (31)$$

Substituting Eqs. (30), (31), and (8) into Eqs. (25) and (26), we find that

$$\begin{aligned} (I_{s/c} + m\ell^2) \ddot{\theta}_{s/c} + m\ell k \cos (\theta_{s/c} - \theta_{sn}) \ddot{\theta}_{sn} + m\ell k \sin (\theta_{s/c} - \theta_{sn}) \dot{\theta}_{sn}^2 \\ + f_h (\dot{\theta}_{s/c} - \dot{\theta}_{sn}) - T_H = F \sin \theta_f \left( - \frac{m\ell \cos \theta_{s/c}}{m_{s/c}} + \ell \cos \theta_{s/c} \right) \\ + F \cos \theta_f \left( \frac{m\ell \sin \theta_{s/c}}{m_{s/c}} - \ell \sin \theta_{s/c} \right) + I_{sx} \ddot{\theta}_x + I_{sy} \ddot{\theta}_y \end{aligned} \quad (32)$$

$$\begin{aligned} (I_{sn} + mk^2) \ddot{\theta}_{sn} + mk\ell \cos (\theta_{s/c} - \theta_{sn}) \ddot{\theta}_{s/c} - mk\ell \sin (\theta_{s/c} - \theta_{sn}) \dot{\theta}_{s/c}^2 \\ + f_h (\dot{\theta}_{sn} - \dot{\theta}_{s/c}) + T_H \\ = F \sin \theta_f \left( - \frac{mk \cos \theta_{sn}}{m_{s/c}} \right) + F \cos \theta_f \left( \frac{mk \sin \theta_{sn}}{m_{s/c}} \right) \end{aligned} \quad (33)$$

Since  $\ddot{\theta}_x$  and  $\ddot{\theta}_y$  are defined to be in the plane of the slewing axis, they are related to the slewing acceleration as follows:

$$\begin{aligned} \ddot{\theta}_x &= R \ddot{\theta}_{slew} \cos \alpha \\ \ddot{\theta}_y &= R \ddot{\theta}_{slew} \sin \alpha \end{aligned} \quad (34)$$

where  $R$  is the ratio of spacecraft acceleration to slewing acceleration defined in Eq. (15) and  $\alpha$  is the angle the slewing axis or axis of revolution makes with the X axis in Fig. 4.

Adding Eqs. (32) and (33) and substituting from Eq. (34), we find that

$$\begin{aligned}
& \ddot{\theta}_{s/c} \left[ I_{s/c} + mkl \cos (\theta_{sn} - \theta_{s/c}) + m\ell^2 \right] \\
& + \ddot{\theta}_{sn} \left[ I_{sn} + mk^2 + m\ell k \cos (\theta_{sn} - \theta_{s/c}) \right] \\
& = F \sin \theta_f \left[ -\frac{m}{m_{s/c}} (k \cos \theta_{sn} + \ell \cos \theta_{s/c}) + \ell \cos \theta_{s/c} \right] \\
& + F \cos \theta_f \left[ \frac{m}{m_{s/c}} (k \sin \theta_{sn} + \ell \sin \theta_{s/c}) - \ell \sin \theta_{s/c} \right] \\
& + \dot{\theta}_{s/c}^2 m\ell k \sin (\theta_{s/c} - \theta_{sn}) - \dot{\theta}_{sn}^2 m\ell k \sin (\theta_{s/c} - \theta_{sn}) \\
& + (I_{xs} R \cos \alpha + I_{ys} R \sin \alpha) \ddot{\theta}_{slew}
\end{aligned} \tag{35}$$

Substituting  $\ddot{\theta}_{s/c} = \ddot{\theta}_{sn}$  as in Eq. (24) and ignoring all products of angular rates as being small relative to the other terms, we find that

$$F = h_{slew} \ddot{\theta}_{slew} \tag{36}$$

The term  $h_{slew}$  is a function of the slewing configuration evaluated in the plane perpendicular to the slewing axis and is evaluated from Eqs. (6) and (7) as follows:

$$h_{slew} = F_x \cos \theta_0 + F_y \sin \theta_0$$

where  $\theta_0$  is the angle between the plane of Fig. 4 and the positive inertial X direction defined in Fig. 2.

The ratio of the inertial spacecraft rate about an axis orthogonal to the slewing rate to the relative scan slewing rate can be evaluated from Eqs. (35) and (36) as follows:

$$\frac{\ddot{\theta}_{s/c}}{\ddot{\theta}_{slew}} = \frac{h_{slew} \left\{ \sin \theta_f \left[ \frac{-m}{m_{s/c}} (k \cos \theta_{sn} + l \cos \theta_{s/c}) + l \cos \theta_{s/c} \right] + \cos \theta_f \left[ \frac{m}{m_{s/c}} (l \sin \theta_{s/c} + k \sin \theta_{sn}) - l \sin \theta_{s/c} \right] \right\} + I_{xs} R \cos \alpha + I_{ys} R \sin \alpha}{I_{s/c} + I_{sn} + m \left[ l^2 + k^2 + 2mk l \cos (\theta_{sn} - \theta_{s/c}) \right]} \quad (37)$$

It will be demonstrated in Section III that the above ratio is accurate to within 10% subject to the limitation that the products of inertia about the spacecraft bus axis perpendicular to the platform axis of revolution are very small or are known accurately.

### III. COMPUTER SIMULATIONS OF MM'71 SCAN PLATFORM DYNAMIC INTERACTION

Extensive computer simulations of the MM'71 attitude control subsystem and spacecraft dynamic interaction prior to launch verified the adequacy of all of the attitude control subsystem designs. The spacecraft-scan platform dynamic interaction was also investigated to evaluate the effect of scan platform dynamic coupling on gas consumption in the celestial cruise mode (Ref. 1).

Based on these simulations, spacecraft performance predictions were prepared to evaluate the observed flight performance. As flight data became available, it was apparent that the predictions did not match the observed performance in the following areas:

- (1) The rates induced in all axes as a result of a scan slew were larger than anticipated.
- (2) The large pitch/yaw plane disturbance resulting from a clock slew was not anticipated.

To resolve the conflict between the predictions and flight observations, two parallel investigations were made. A dynamic analysis (presented in Section II) and a dynamic simulation were constructed which modeled the spacecraft bus and scan platform as two rigid bodies connected by a two-degree-of-freedom hinge. The dynamic equations of motion in the two-body

simulation are solved by a computer subroutine MLTBDY (Ref. 2) developed to study spacecraft with multiple rigid parts connected by hinged spring/damper systems. The results of the analysis and computer simulations both agreed closely with the observed flight data.

This section will outline the development of the scan actuator model, compare the model response to the simulated response, and demonstrate the accuracy of the computer simulation and analysis techniques.

#### A. Scan Platform Dynamic Model Development

A typical scan slew consists of a clock slew, followed 1 s later by a cone slew. Each slew is performed in 0.25-deg increments once a second. The on-board computer orders the clock or cone axes to step 0.25 deg by sending a command to a sequencing circuit, which issues four commands to a stepper motor causing it to rotate one complete revolution. The stepper motor drives a reference potentiometer, which provides the error signal to the scan actuator servo motor. The stepper motor actuation sequence, the scan platform response, and the dynamic actuator model used to model the stepper motor gear train and scan platform are illustrated in Fig. 5.

A simple spring/viscous damper model was sought which would accurately model the servo motor gear train feedback loop.

The scan control system design documentation (Ref. 3) and a subsequent dynamic analysis (Ref. 2) describe a scan servo-load analysis similar to that presented in Appendix A. The linearized scan control system block diagram based on this analysis is shown in Fig. 6a. The simulated platform displacement resulting from a 0.25-deg step command is illustrated by curve 2 in Fig. 7.

The measured actuator shaft displacement without the platform load for a 0.25-deg step command is shown as curve 1 in Fig. 7. The close agreement between the analytical model displacement and the measured actuator displacement apparently validated the analytical model. The structure of the simulation program and the analytic expressions required that the displacement of the scan platform be determined as a function of the platform inertia  $J_1$ , a spring constant  $K_h$ , and a viscous damping coefficient  $f_h$ , as illustrated in Fig. 6b. The mechanical stiffness of the actuator mechanism was evaluated in static deflection tests and proved to be a

nonlinear function of displacement. For small deflections, the nonlinear stiffness was approximated as 4068 N-m/rad. Since the platform inertia was known, a complete model could be constructed with the selection of a damping coefficient such that the scan displacement determined from the actuator model was reproduced. A series of single-axis simulations quickly converged to a viscous damping coefficient of about 678 N-m/rad/s.

A series of simulations of MM'71 gas consumption anomalies related to the scan platform dynamic interaction with the spacecraft (discussed in Section III-B) revealed that the peak spacecraft rates resulting from a 0.25-deg platform displacement were much greater than predicted by the existing models. Reducing the viscous damping coefficient in the dynamic simulations from 678 to 407 N-m/rad/s produced the desired spacecraft rate disturbances, but the platform displacement characteristics illustrated by curve 3 in Fig. 7 differed significantly from other model predictions (curve 2) and preflight actuator displacement measurements (curve 1).

It was determined that previous analyses and modeling had ignored the displacement in the actuator gear train in determining the position of the feedback potentiometer. When this effect was considered in the analysis (see Appendix B for details), the scan control system linear servo block diagram presented in Fig. 6c resulted. The relative platform displacement using this model is illustrated by curve 4 in Fig. 7. The relative platform angular rates corresponding to curves 2, 3, and 4 in Fig. 7 are shown by curves 2, 3, and 4, respectively, in Fig. 8. The peak-to-peak platform rate must be at least 0.032 rad/s to cause the observed spacecraft disturbance. The initial scan control system model rate, curve 2 in Fig. 8, reaches a peak rate of only 0.015 rad/s. The model used in the dynamic simulations, curve 3 in Fig. 8, does have the required rate increment but is a conservative model if the 0.035-rad/s peak-to-peak rates implied by curve 4 are closer to the actual platform rates.

It is concluded that the simplified spring/mass/damper model (Fig. 6b) is desirable in the digital computer model to reduce the run time expense and at the same time, provide all the dynamic characteristics necessary for detailed analysis and evaluation.

## B. Scan Platform Dynamic Interaction Computer Simulation Results

The MM'71 mission revealed that the existing scan interaction model did not accurately predict spacecraft flight performance. For example, 8 days after orbit insertion, the spacecraft Canopus tracker experienced straylight interference from the small Martian moon, Phobos. To prevent loss of the roll celestial reference during the disturbance periods, the spacecraft was placed in the roll-axis inertial mode. However, during the periods of roll-axis inertial operation and clock-axis slewing, an excessive amount of attitude control gas was used. The existing scan platform slewing simulations with a damping coefficient of 678 N-m/rad/s did not indicate that a gas consumption problem existed, but additional simulations with a reduced equivalent viscous damping coefficient of about 406.8 N-m/rad/s did reproduce the observed flight gas consumption.

The magnitude of the observed spacecraft rate disturbance is a function of the actuator stiffness and viscous damping coefficients. As the damping coefficient is decreased, the peak spacecraft rate disturbance is increased, although the average spacecraft rate remains a fixed function of the constant average slewing rate. The gas used during a clock-axis slew must be evaluated for two separate cases.

In the first case, the peak spacecraft rate disturbance resulting from a 0.25-deg clock step exceeds the roll-axis rate plus position deadband each scan step. In this case (Fig. 9), the rate increment is positioned such that the average spacecraft rate is about zero, but the gas jets are fired in one direction during the slew transient and the other direction when the transient dies out. The gas consumption in this mode is about  $0.021 \times 10^{-3}$  kg per clock-axis step.

In the second case, the peak spacecraft roll rate induced during a clock-axis slew is less than the total rate deadband. In this mode of operation, the gas consumption in the roll-axis inertial mode is directly proportional to the peak spacecraft rate resulting from a clock-axis scan slew. Initially, the peak induced spacecraft rates are forced by gas jet firings to be constrained within the rate deadbands, as illustrated in Fig. 10. The gas consumption during this period can be estimated by

$$GT = \frac{2\dot{\theta}_{ss}}{\dot{\Delta\theta}} W_p$$

where

$\dot{\theta}_{ss}$  = peak spacecraft rate resulting from a scan slew

$\dot{\Delta\theta}$  = spacecraft rate increment per gas jet pulse  $\approx (30 \times 10^{-6} \text{ rad/s})$

$W_p$  = gas weight per pulse

After the average spacecraft rate is brought to within a single gas jet pulse of zero rate, the time between gas jet pulses is also a function of the peak slew induced spacecraft rate. The gas consumption can be evaluated if the following conditions are satisfied:

- (1) The spacecraft peak rate disturbance due to a scan slew is less than the total rate deadband.
- (2) The spacecraft position is such that no gas jets fire between scan steps.
- (3) The average spacecraft rate is within one gas jet pulse at zero spacecraft rate.

When the above conditions are satisfied, the operational position deadband width can be evaluated by

$$\theta_{es} = (2\dot{\theta}_{db} - \dot{\theta}_{ss})T_{rp}$$

where

$\theta_{es}$  = the equivalent position deadband width during steady-state scan slewing in the inertial mode

$\dot{\theta}_{db}$  = the rate magnitude which causes the gas jets to fire when the spacecraft position is at null  $= 356 \times 10^{-6} \text{ rad/s}$

$T_{rp}$  = the rate-to-position gain in the rate-plus-position mode during scan slewing = 4.23 s

The gas consumption in this operating mode can be conservatively estimated by

$$GR = \frac{GP \Delta \dot{\theta}}{\theta_{es}}$$

where

GR = the gas consumption rate during scan slewing in the inertial mode after the initial transient is removed in kg/s

GP = the gas use per gas jet firing  $\approx 7.07 \times 10^{-6}$  kg/pulse

For a viscous damping coefficient of 542.4 N-m/rad/s, the peak spacecraft rate disturbance is 400  $\mu$ rad/s. For this case, the steady-state slewing gas consumption in the roll inertial mode is about  $1.58 \times 10^{-7}$  kg/step.

During the initial MM'71 Phobos interference periods, about 2000 0.25-deg clock steps were taken in the roll inertial, mode and an excess of about  $41 \times 10^{-3}$  kg of gas was used. Clearly, the damping coefficient must have been in the neighborhood of  $407 \times 10^{-3}$  N-m/rad/s to explain the observed flight gas consumption.

To further verify the modeling technique, an actual flight slewing sequence on GMT 056:08:03 was simulated, and the results were compared to spacecraft flight telemetry data.

The spacecraft pitch, yaw, and roll position telemetry values are plotted in Fig. 11 and compared to the results of a computer simulation. The initial rates in the simulation are to be the same as the spacecraft's, and the initial positions at slew start are very close, except in the yaw axes. The pitch and roll simulated position errors are almost identical to the observed flight data, except that the flight derived rate damping appears to be better than the simulated derived rate damping.

The yaw-axis simulated initial position is offset slightly from the spacecraft position, but this should have negligible impact on the simulated position error signal characteristics. The yaw position error indicates the presence of a small positive disturbance torque that is slightly larger in the simulation than on the actual spacecraft. The difference between the torque

magnitude observed in the simulation and actual flight data is very small and is probably the result of errors in the spacecraft inertia and center-of-mass estimates used in the simulation.

In summary, the two-body computer simulation very closely reproduced the observed MM'71 flight performance. Had this simulation method been in existence prior to the flight, scan control system design changes or at least, operational changes, would have been made. The fact that actual flight situations have been accurately simulated should provide the reassurances necessary to make multi-rigid-body simulations the principal design and evaluation tool in scan actuator and control system design.

#### IV. ANALYTICAL EVALUATION OF MM'71 SCAN PLATFORM DYNAMIC INTERACTION

The following discussion uses the analytical technique developed in Section II to evaluate the MM'71 spacecraft scan platform dynamic interaction. The objective of this effort is to verify that the analytical methods developed here can be used to determine, with reasonable accuracy, the pertinent spacecraft dynamic information needed for scan platform and actuator design and evaluation. Each parameter used in the development of Eqs. (1) through (37) will be defined for both the clock and cone scan platform slewing axes, and the ratio of accelerations about the axis of revolution and due to the reaction forces will be determined.

##### A. Cone-Axis Scan Platform Slewing Configuration and Disturbances

###### 1. Axis of revolution configuration and disturbances (cone slew).

The MM'71 scan platform cone-axis configuration is illustrated in Fig. 1. The cone axis of revolution is perpendicular to the plane of the paper, and has the following location in the spacecraft bus coordinate system:

$$R_h = 0.0015 \text{ m}$$

$$Y_h = -0.076 \text{ m}$$

$$R_h = 0.637 \text{ m}$$

With the aid of Fig. 1 and Table 1, it is possible to determine the relationships that describe the variables used in Eqs. (1) through (15) in terms of celestial position error angles and the scan platform clock and cone positions during a cone slew.

Substituting the values obtained in Eq. (15) reveals that the ratio of the spacecraft rate or acceleration to the scan slewing rate or acceleration is -0.0455 for a cone slew. Appendix C demonstrates a method of determining the approximate relative scan slewing rate as a function of time. The analysis also evaluates the peak relative scan slewing rate during a 0.25-deg scan slew to be about 0.0326 rad/s. Multiplying the ratio of spacecraft rate to scan slewing rate by the peak scan slewing rate indicates that the peak spacecraft rate observed in the pitch-yaw plane during a cone slew will be about  $1.482 \times 10^{-3}$  rad/s.

Fig. 12 illustrates the simulated pitch-, and yaw-, and roll-rate disturbance during two 0.25-deg cone-axis steps. The peak pitch-yaw plane disturbance is determined to be  $1.440 \times 10^{-3}$  rad/s from the simulation and agrees within 5% with the analytical determination.

2. Configuration and disturbances in the axis orthogonal to the cone slewing axis. The MM'71 scan platform has two orthogonal degrees of freedom. The axis orthogonal to the cone axis is the clock axis. The clock-axis configuration is illustrated in Fig. 13. With the aid of Fig. 13 and Table 1, it is possible to determine the relationships that describe the variables used in Eqs. (24) through (37) in terms of celestial position error angles and the scan platform clock and cone angles during a cone-axis slew.

Substituting the values obtained into Eq. (37) reveals that the ratio of spacecraft rate or acceleration about the clock axis to the cone axis rate or acceleration is -0.001106. The peak cone-axis rate, as determined from the relations in Appendix C, is 0.0326 rad/s so that the evaluated peak roll rate is  $36 \times 10^{-6}$  rad/s. Figure 13 shows that the peak roll rate for two 0.25-deg cone steps is  $37 \times 10^{-6}$  rad/s, well within a 5% error tolerance.

## B. Clock-Axis Scan Platform Slewing Configuration and Disturbances

1. Axis of revolution configurations and disturbances (clock slew). The MM'71 scan platform clock-axis configuration is illustrated in Fig. 13.

The clock axis is perpendicular to the plane of the paper and has the same coordinate location in the spacecraft coordinate system as the cone axis.

With the aid of Fig. 13 and Table 1, it is possible to determine the relationships that describe the variables used in Eqs. (1) through (15) in terms of celestial error angles and the scan platform clock and cone positions during a clock-axis slew.

Substituting the values obtained in Eq. (15) reveals that the ratio of spacecraft rate or acceleration to the scan slewing rate or acceleration is -0.0214. Appendix C describes the method for determining the approximate relative scan slewing rate as a function of time. The peak slewing rate determined from this analysis is 0.0313 rad/s. Multiplying the ratio of spacecraft rate to scan slewing rate by the peak scan slewing rate indicates that the peak spacecraft roll rate during a clock slew will be about  $672 \times 10^{-6}$  rad/s. Figure 14 illustrates the simulated pitch, yaw, and roll rate disturbances during two 0.25-deg clock-axis steps. The peak roll-axis rate is observed to be  $700 \times 10^{-6}$  rad/s from the simulation and agrees within 5% with the analytical determination.

2. Configuration and disturbances in the axis orthogonal to the clock slewing axis. The scan platform cone axis is orthogonal to the clock axis. The cone axis configuration and variable definitions are illustrated in Fig. 1. Substituting the variable values determined from Fig. 1 and Table 1 into Eq. (37) reveals that the ratio of spacecraft rate or acceleration about the cone axis to the clock-axis rate or acceleration is -0.02058. The peak clock-axis rate, as determined from the relations in Appendix C, is 0.0313 rad/s, so that the evaluated peak spacecraft rate around the cone axis is  $644.0 \times 10^{-6}$  rad/s (assuming negligible products of inertia). The cone axis lies in the pitch-yaw plane, so that the peak spacecraft rate disturbance around the cone axis can be resolved into components along the pitch and yaw axes. For the clock slew simulated in Fig. 14, the evaluated pitch maximum rate is  $381 \times 10^{-6}$  rad/s, and the maximum yaw rate is  $521.7 \times 10^{-6}$  rad/s. The evaluated peak pitch rate differs from the simulated rate by  $50 \times 10^{-6}$  rad/s, or about 12%. The evaluated peak yaw rate differs from the simulated rate by  $90 \times 10^{-6}$  rad/s, or about 20%. The large evaluation error resulted because the products of inertia about the

cone axis were significant but unknown and were assumed to be zero for the evaluation. Therefore, accurate evaluation of the disturbances in axes orthogonal to the slewing axis must be limited to those cases in which the products of inertia are small or are known accurately.

## V. ATTITUDE CONTROL GAS CONSUMPTION RESULTING FROM THE FORCED RELATIVE MOTION OF TWO BODIES IN SPACE

When two bodies move relative to each other in space in the absence of external disturbances, a corresponding change in the inertial position of both bodies is required so that the composite center of mass of the two bodies does not move in the inertial frame. This principle is illustrated in Fig. 15. When the position displacement of a three-axis-controlled spacecraft exceeds the deadband values, the gas jets fire in an attempt to keep the position errors within the specified pointing allowance. The object of this section is to outline guidelines which will enable analysts to determine (on the average) the amount of attitude control gas that will be used for a given platform-spacecraft configuration, slewing rate, slew size, and attitude control system.

The principal step in determining the attitude control system gas usage during a scan slew is to evaluate the average momentum imparted to each spacecraft axis as a function of the average slewing rate. The amount of gas used in each axis is proportional to the average momentum imparted to that axis and the duration or length of the slew. The analytical tools to accomplish the above evaluations will be developed in this section, and examples of MM'71 scan platform gas consumption evaluations will be presented.

### A. Determination of the Angular Momentum in Each of the Three Spacecraft Axes as a Result of the Forced Relative Motion of Two Bodies

When two bodies move relative to each other in space, the average induced spacecraft bus rate about the axis of relative motion or revolution can be evaluated using Eq. (15), the ratio of the spacecraft rate to the scan slewing rate. For example, the evaluated MM'71 ratio of spacecraft rate to clock-axis slewing rate was determined to be -0.0214. The commanded

slewing rate is a constant 0.0044 rad/s, so that the average spacecraft rate about the clock axis is  $94.2 \times 10^{-6}$  rad/s.

The disturbance in the axis orthogonal to the slewing axis is determined from Eq. (37), the ratio of the spacecraft rate about an axis orthogonal to the slewing axis to the slewing rate. For example, the MM'71 ratio of the spacecraft rate in the spacecraft pitch-yaw plane to the clock-axis slewing rate was calculated to be -0.02058. The average clock-axis rate is 0.0044 rad/s, so that the average spacecraft rate in the pitch-yaw plane is  $90.6 \times 10^{-6}$  rad/s. Both of these average rates can be verified in Fig. 14 by evaluating the average slope of the spacecraft position error values during a 0.25-deg clock-axis step.

In the cone axis, the evaluated MM'71 ratio of spacecraft rate to cone slewing rate was determined to be -0.0455. The commanded slewing rate is 0.0044 rad/s, and so the average spacecraft rate about the cone axis is  $198 \times 10^{-6}$  rad/s.

The disturbance in the axis orthogonal to the slewing axis is determined from Eq. (37), the ratio of the spacecraft rate about an axis orthogonal to the slewing axis to the slewing rate. For example, the MM'71 ratio of the spacecraft rate about the roll axis to the cone-axis slewing rate was calculated to be -0.001106. The average cone axis rate is 0.0044 rad/s, so that the average roll-axis rate resulting from a cone slew is  $4.8 \times 10^{-6}$  rad/s. Both of these average rates can be verified in Fig. 12 by evaluating the average slope of the spacecraft position error values during a 0.25-deg cone-axis step.

B. Determination of the Gas Required to Remove the Angular Momentum Resulting From the Forced Relative Motion of Two Bodies

The amount of attitude control gas used during any appendage movement is a function of

- (1) The average and peak magnitude of the angular momentum imparted to each axis. (This is a function of the slewing rate.)
- (2) The duration of the slew.
- (3) The attitude control implementation or mode.

An important factor in evaluating the amount of gas that will be used during appendage slewing is the attitude control implementation or mode. For example, each controlled axis on MM'71 used a bang-bang system with a deadband and derived-rate feedback. No gas jets were fired until the deadband was exceeded, and then the gas jets were constrained to a duty cycle of less than 10%. The result of this type of control is a position hang-off which may exceed 2 mrad if the scan slew is long enough (Fig. 16a). However, the slews generally required less time than that required to reverse the average rate disturbance due to slewing and resulted in a gas saving (see Fig. 16b).

This performance may be compared to MM'71 slewing in the inertial mode demonstrated in Fig. 9. In this mode, the gas consumption is proportional to the peak induced spacecraft rate and is much greater than in the derived-rate mode.

Future spacecraft may require slewing in the inertial mode or have rate estimators that are not disabled during slewing. In such cases, the gas consumption is a function of the peak spacecraft rate in each axis and can be determined using the methods described previously. In general, however, scan slewing will be done in the celestially oriented mode, with the rate estimator or gyro rate information disabled to the switching amplifier while the spacecraft position error is within the position deadbands. In this mode, the average gas consumption is proportional to the slew length up to some maximum value.\*

The maximum amount of gas used in each axis during any slew is

$$W_{gmax} = \frac{2M DF}{L I_{sp}} \quad (38)$$

where

$I_{sp}$  = specific impulse of the attitude control gas (68 s for MM'71)

$M$  = average momentum imparted to the spacecraft axis in question during a slew

---

\*The systematic method of evaluating gas consumption due to scan slewing presented here was first outlined by R. S. Edmunds (Ref. 4).

L = length of the gas jet lever arm about the axis in question

DF = damping factor of the attitude control system in the axis in question

The damping factor is the ratio of the absolute value of the sum of the average spacecraft rate coming into a spacecraft deadband before the gas jets are fired and the spacecraft rate coming back into the position deadbands after the gas jet firings to the average spacecraft rate before the gas jets are fired. This ratio is expressed by

$$DF = \left| \frac{\dot{\theta}_b + \dot{\theta}_a}{\dot{\theta}_b} \right| \quad (39)$$

where

$\dot{\theta}_b$  = spacecraft rate before gas jet firings (see Fig. 16)

$\dot{\theta}_a$  = spacecraft rate after gas jet firings.

The MM'71 damping factor was about 1.3 in all axes. The factor 2 in Eq. (38) accounts for the fact that if slewing momentum is removed from the spacecraft with gas jets during a slew, it must be returned to the spacecraft after the slew is completed, as illustrated in Fig. 16a. The maximum amount of gas is used in each axis if the slew lasts for  $t_g$  seconds after the deadband has been exceeded. This number is a function of the attitude control strategy. On MM'71, a derived-rate system was used which limited gas jet pulsing to about one pulse every 2.2 s. Therefore,  $t_g$  may be evaluated in each axis by

$$t_g = \frac{\dot{\theta}_a}{\dot{\theta}_p} P_r \quad (40)$$

where

$\dot{\theta}_a$  = average spacecraft rate induced during a slew

$\dot{\theta}_p$  = spacecraft rate due to one gas jet pulse

$P_r$  = maximum gas jet pulse rate in the control mode existing during slewing

Table 2 lists the MM'71 values of  $t_g$  for both clock and cone slews. The position deadband in a given spacecraft axis will always be exceeded if a slew lasts for  $t_t$  seconds. The value of the maximum transit time ( $t_t$ ) is

$$t_t = \frac{\theta_{db}}{\dot{\theta}_a} \quad (41)$$

where  $\theta_{db}$  = the position deadband width.

The MM'71 transit time values are listed in Table 2. The gas consumption for a given slew magnitude can now be calculated as follows (where  $t_s$  = slew duration):

Case 1

$$0 < t_s < t_g$$

$$W_g = W_{gmax} K_0$$

$$K_0 = \frac{\dot{\theta}_a t_s}{\theta_{db}} \quad (42)$$

Case 2

$$t_g < t_s < t_t$$

$$W_g = W_{gmax} K_1$$

$$K_1 = \frac{\dot{\theta}_a t_s}{\theta_{db}} \quad (43)$$

### Case 3

$$t_t < t_s < t_t + t_g$$

$$W_g = W_{gmax} K_2$$

$$K_2 = \frac{t_s}{(t_t + t_g)} \quad (44)$$

### Case 4

$$t_t + t_g < t_s$$

$$W_g = W_{gmax} \quad (45)$$

The values of the various Mariner gains (K) are given in Table 2.

A method similar to the one described above (Ref. 4) was used to calculate the MM'71 gas consumption for 10 high-activity orbits. The values obtained in this evaluation closely matched the observed gas consumption.

### C. Summary and Conclusions

In this section, a method of estimating the amount of attitude control gas consumed in a given scan slew has been proposed. This method assumes that the approximate spacecraft rate at slew start is zero, and the spacecraft position at slew start has an equal probability of being anywhere in the position deadband. Most slewing sequences have many slews close together, so that only a small percentage of the slews may be considered independent. However, MM'71 experience indicates that each slew may be considered independent for gas consumption evaluations and will provide reasonably accurate long-term gas usage estimates.

## VI. DESIGN AND CONTROL OF ARTICULATED SPACECRAFT PLATFORMS

The configuration, location on the spacecraft bus, and control of articulated spacecraft packages such as scan platforms, antennas, solar panels, etc., should be accomplished as a combined effort with a common objective. Unfortunately, many times the articulated package is configured independent of its actuating mechanism, and the actuating mechanism and control strategy are a compromise selected for economy or versatility. The purpose of this section is to establish a consistent set of design objectives compatible with all facets of design and control of articulated spacecraft packages. As examples, guidelines will be recommended in

- (1) Package configuration and location on the spacecraft.
- (2) Actuator mechanism capabilities and control system design.

### A. Design Objective

When one body is forced to move relative to another in space, a dynamic interaction occurs, as described earlier, and electrical power is required. Minimizing these disturbances to the spacecraft usually results in other design benefits or advantages. For example, minimum power requirements usually imply minimum actuator size and weight, and a minimum dynamic disturbance implies that a minimum amount of attitude control gas will be required to achieve the desired level of control.

It is regrettable that the most desirable designs in all subsystems must be compromised for economy and development reasons. However, this compromise should not alter the idealized design objectives, only the implementation schemes. The following objectives are proposed in the design of articulated packages and their actuator mechanisms:

- (1) Satisfy the package articulation requirements, such as
  - (a) Field of view.
  - (b) Accuracy of pointing.
  - (c) Rate of pointing.
- (2) Minimize the disturbance resulting from the articulation on all spacecraft subsystems.

In the actual design of an articulated package and control system, the above objectives must be evaluated within the framework of a specific spacecraft design. For example, in a given design, power allocations to the articulation control system may be generous, or short-duration, large rate disturbances may not have any impact on the attitude control subsystem or expendable gas consumption. In cases like these, it is desirable but not necessary to follow the guidelines presented in the following sections.

#### B. Design and Location of Articulated Spacecraft Packages

It is assumed that two basic types of articulated packages exist on the spacecraft. The first type has a fixed configuration such as an antenna, but location of the actuator mechanism is flexible; the second has many small components with a flexible center of mass and actuator configuration, such as the science instrument platform. Each of these articulated packages may have more than one degree of freedom, but the design guidelines are the same in all cases.

This section outlines the articulated package configuration design guidelines for the two basic steps in articulated package design:

- (1) Design of the package configuration.
- (2) Location of the package on the spacecraft.

The articulated package includes all components that must move relative to the spacecraft bus structure. Equation (15) reveals that the spacecraft dynamic disturbances about axes parallel to the axis of revolution are minimized if the distance from the actuator axis of revolution to the package center of mass,  $k$ , is minimized (see Fig. 2). Ideally, the axis of revolution for all degrees of freedom should pass through the package center of mass. When the package is located on the spacecraft bus and  $k$  is not zero, all torques resulting from the reaction forces at the hinge are minimized if the distance from the effective actuator hinge point to the spacecraft center of mass is selected as small as possible. In Eqs. (15) and (37) and Figs. 2 and 4, this is equivalent to minimizing  $l$ .

### C. Articulated Package Actuator and Controls Design Guidelines

The actuator is the electromechanical link between the spacecraft and the articulated package. In general, it is desirable to make this link as stiff as possible to keep the natural frequency of the spacecraft-actuator package as high as possible and therefore minimize any possible interference with the low-frequency spacecraft attitude control system. The spectrum of possible actuator designs and control concepts is so broad that specific recommendations are futile. In general, however, the design which minimizes the articulated package acceleration relative to the spacecraft bus will minimize disturbances to the spacecraft bus structure.

### D. Guideline Summary

The MM'71 scan platform actuator and control system will be evaluated here relative to each of the guidelines drawn in the preceding paragraphs.

The now historic record of MM'71 indicates that the scientific instruments had an adequate field of view, were pointed accurately, and the 0.25-deg/s slewing rate was satisfactory. It has also been demonstrated that scan slewing power requirements were reasonable and were never the determining factor in operational strategy decisions.

The scan platform's center-of-mass location relative to the platform axes of revolution left much to be desired. The cone axis of revolution was displaced from the scan platform center of mass by 0.3 m. The clock axis of revolution displacement from the scan center of mass was a function of the cone angle, with a mean value of about 0.26 m.

The platform was located as close to the spacecraft center of mass as configuration limitations allowed. The actual hinge point was still in excess of 0.61 m from the spacecraft bus center of mass. This large lever arm was the mechanism which caused the large pitch- and yaw-axis disturbances during a clock-axis slew. Conversely, the negligible roll disturbance resulting from a cone slew was the consequence of a very short lever arm from the cone axis of revolution to the axis parallel to the roll axis, originating at the spacecraft bus center of mass.

The scan actuator and control system design analyses (Ref. 4) and preflight tests indicated that the relative scan displacement was more than

critically damped and would have resulted in a very small peak spacecraft rate disturbance, but flight performance indicated otherwise. It is impossible to determine whether a modeling oversight actually occurred, but a more comprehensive preflight testing program might have eliminated the existing doubts.

## VII. CONCLUSION

The multi-rigid-body computer simulations of the MM'71 scan platform/spacecraft bus dynamic interaction agreed very closely with the observed flight performance.

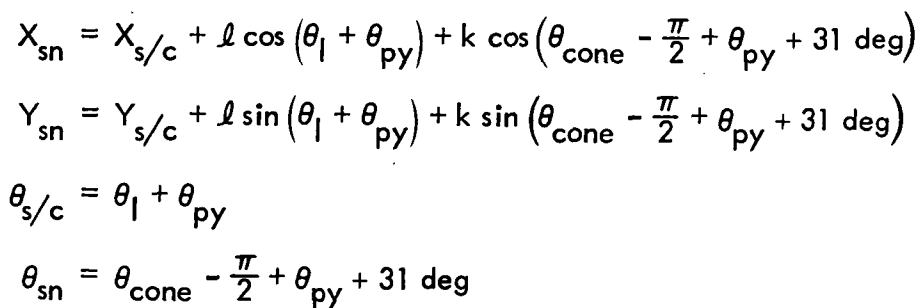
The analytical expressions derived also proved to be a rapid and accurate method of bounding the slewing disturbance observed by the spacecraft and evaluating attitude gas consumption. In the future, the analytic methods and computer simulation techniques presented here could also provide the insight and tools needed to improve articulated platform design and control.

Table 1. MM'71 scan-axis  
parameter evaluation

Parameter	Cone Axis	Clock Axis
$m_{sn}$ , kg	74.42	
$m_{s/c}$ , kg	3502.5	
$I_{s/c}$ , kg m <sup>2</sup>	$317.2 + 24.8 \sin (\theta_{cl} - 122 \text{ deg})$	458.8
$I_{sn}$ , kg m <sup>2</sup>	2.98	$7.3 \left  \cos (\theta_{cone} + 31 \text{ deg}) \right $
$k$ , m	0.2977	$0.297 \sin (31 \text{ deg} + \theta_{cone})$
$l$ , m	$\sqrt{0.61^2 + \left[ 0.076 \cos \theta_{cl} - 56.8 \right]^2}$	0.076
$\theta_{sn}$	$(\theta_{cone} + 31 \text{ deg}) - 90 \text{ deg} + \theta_{py}$	$360 \text{ deg} - (\theta_{cl} + \alpha) + \theta_r$
$\theta_{s/c}$	$\theta_{py} + \theta_1$	$\phi - \alpha + \theta_r$
$\theta_1$ , deg	86	
$\phi$ , deg		303.2

Table 2. MM'71 slewing gas consumption parameter definitions

Inertia, kg m <sup>2</sup>	Slew	Axis	Average induced spacecraft rate $\dot{\theta}_a$ , rad/s	$\dot{\theta}_p$ , rad/s $\times 10^{-6}$	$t_g$ , s	$t_t$ , s	$W_{gmax}$ , kg $\times 10^{-3}$	$\frac{K_0}{t_s}$	$\frac{K_1}{t_s}$	$\frac{K_2}{t_s}$
325	Cone	Revolution	$198 \times 10^{-6}$	17	26	44	0.875	0.0225	0.0225	0.0143
470	Cone	Orthogonal	$4.8 \times 10^{-6}$	30	0.4	1833	0.03	0.0005	0.0005	0.0005
458	Clock	Revolution	$94 \times 10^{-6}$	30	7	94	0.589	0.011	0.011	0.0099
380	Clock	Orthogonal	$90 \times 10^{-6}$	17	12	98	0.46	0.010	0.010	0.0091



JPL Technical Memorandum 33-624

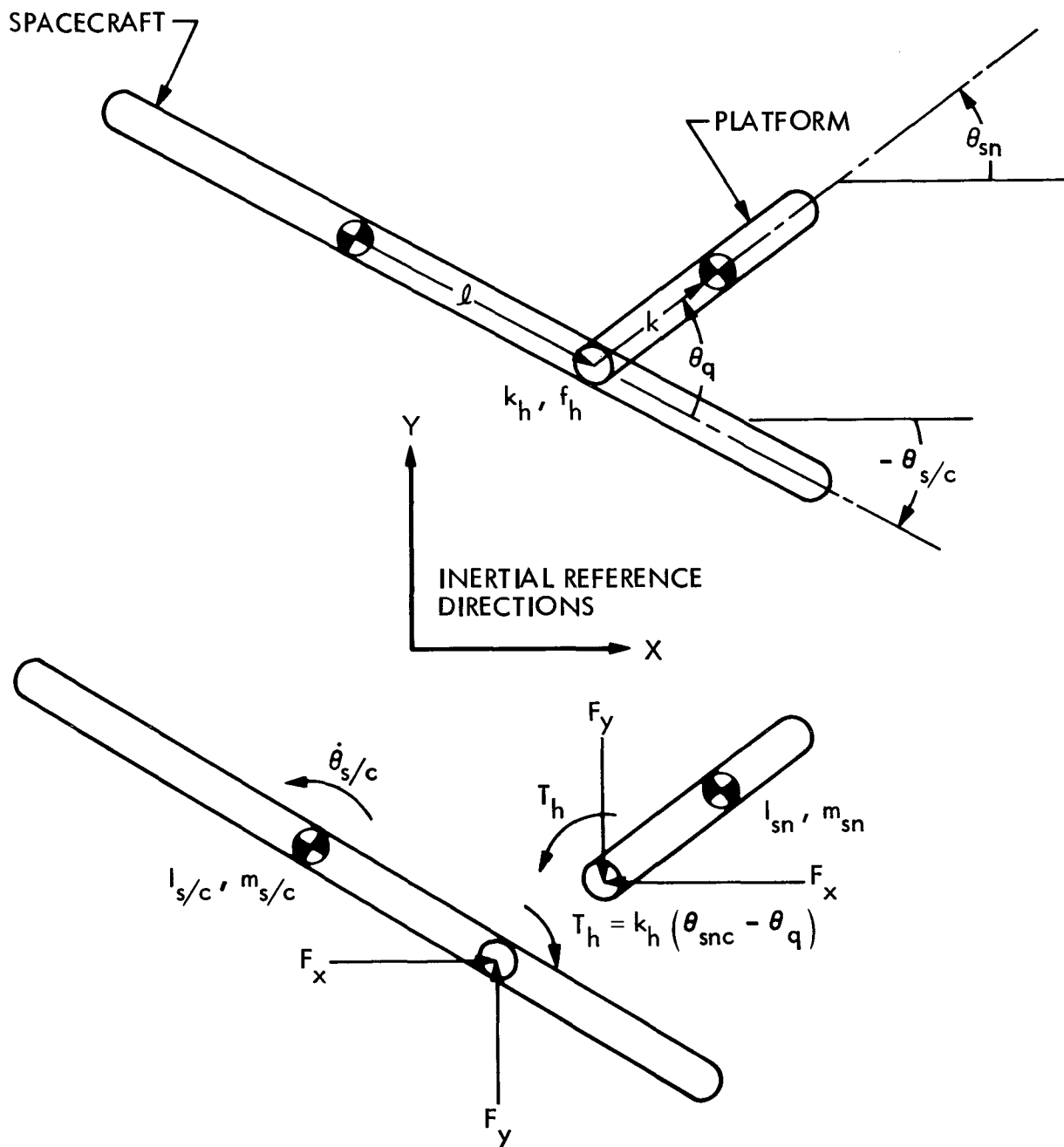


Fig. 2. Simplified spacecraft bus and platform configuration and free-body diagram

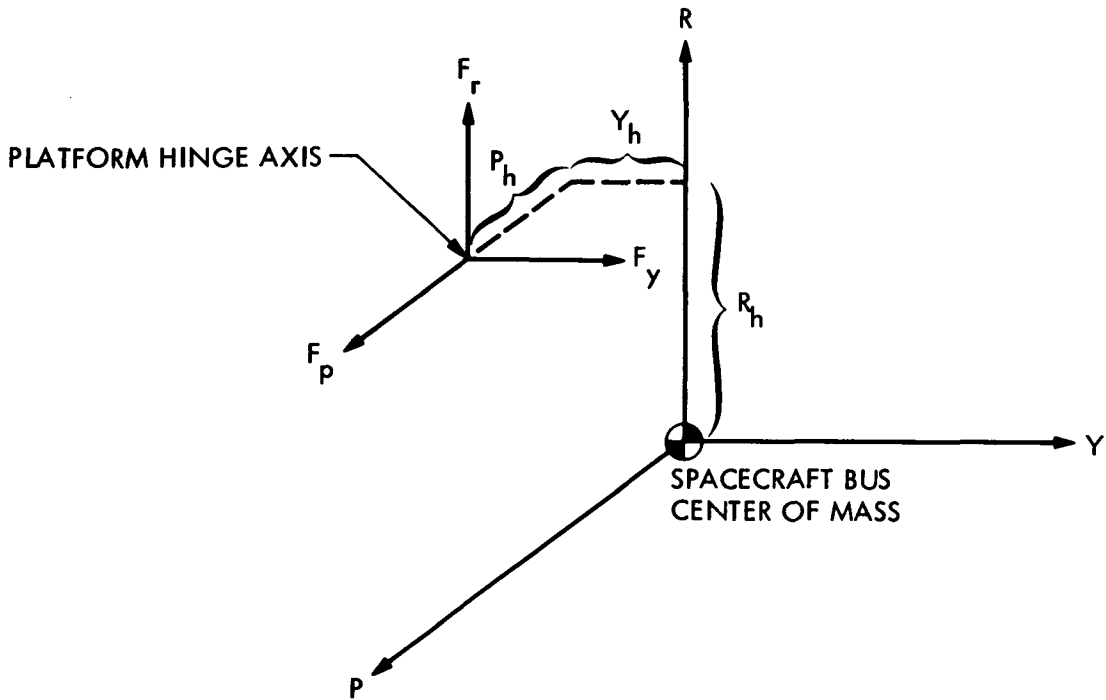


Fig. 3. Spacecraft mass-centered coordinate system and scan hinge point

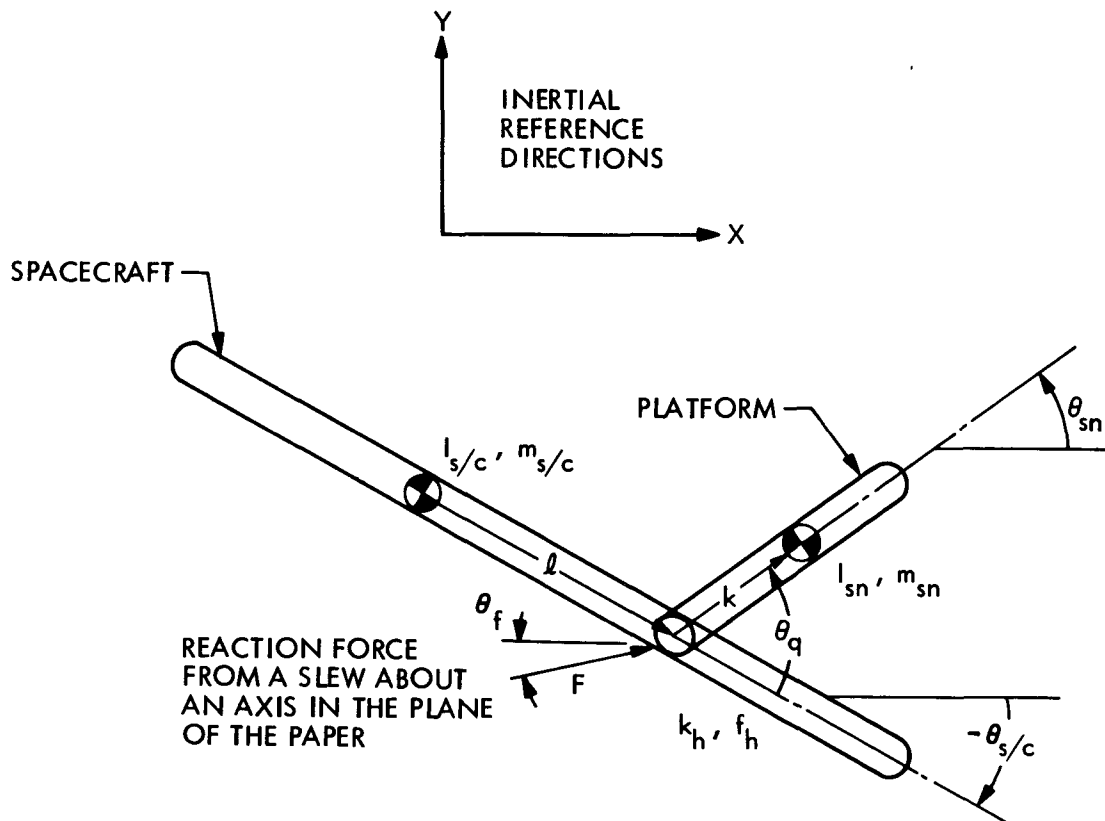


Fig. 4. Spacecraft/platform model with reaction force from a scan slew

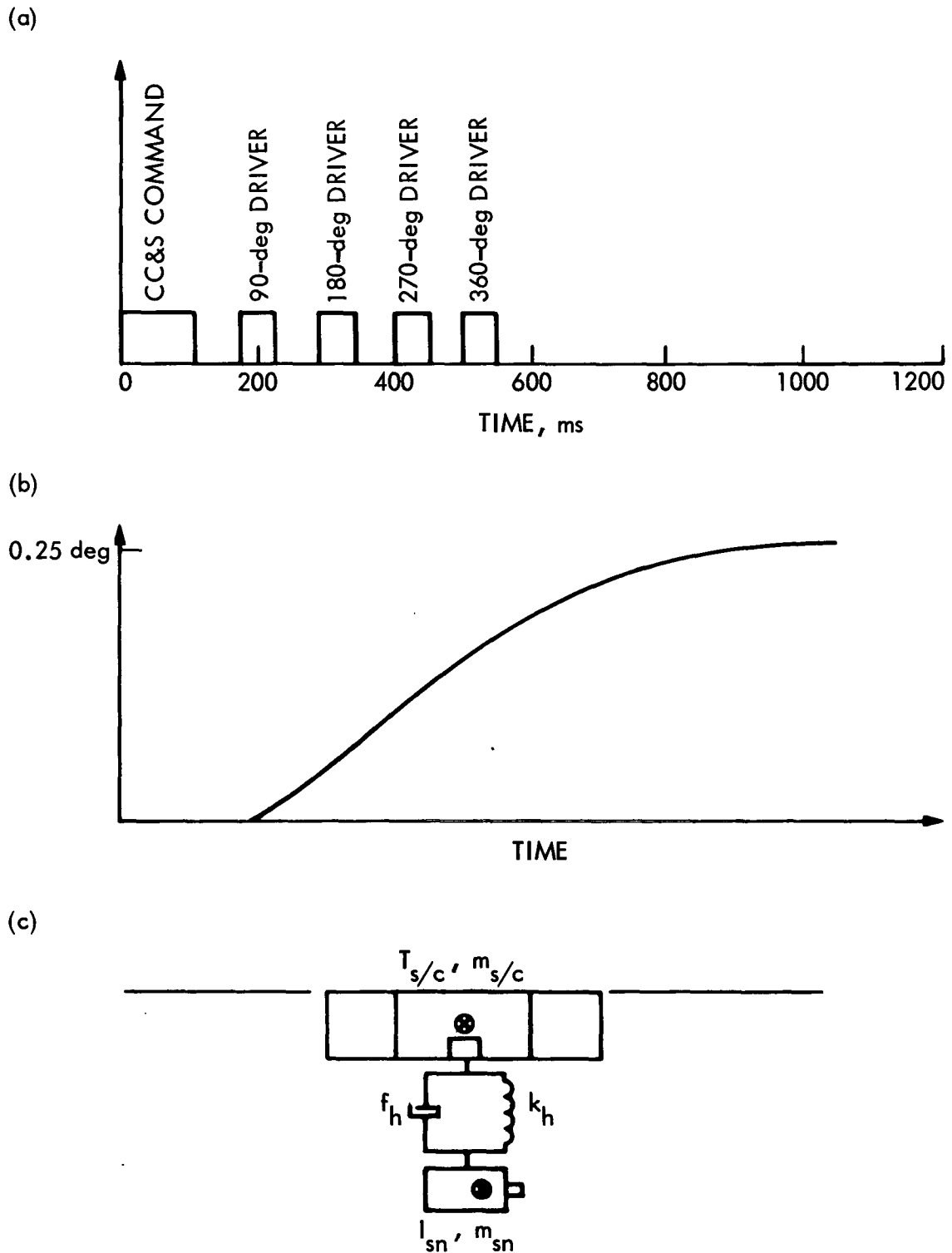


Fig. 5. Scan platform model development components: a. Logic sequence for scan stepper motor commands, b. Scan actuator displacement, c. Scan actuator model

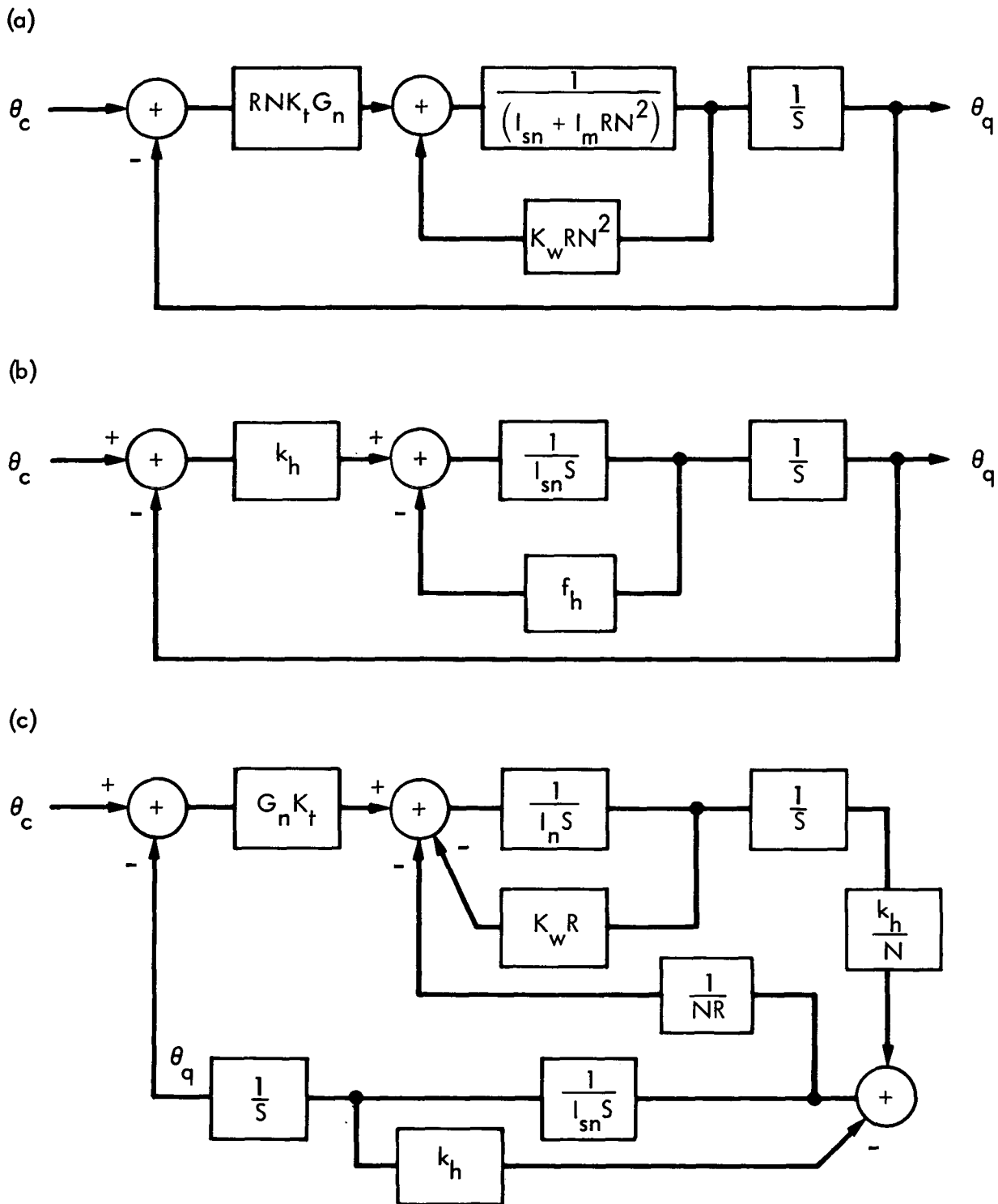


Fig. 6. Scan platform dynamic models: a. Scan control linear servo, b. Scan spring/mass/damper, c. Improved scan linear servo

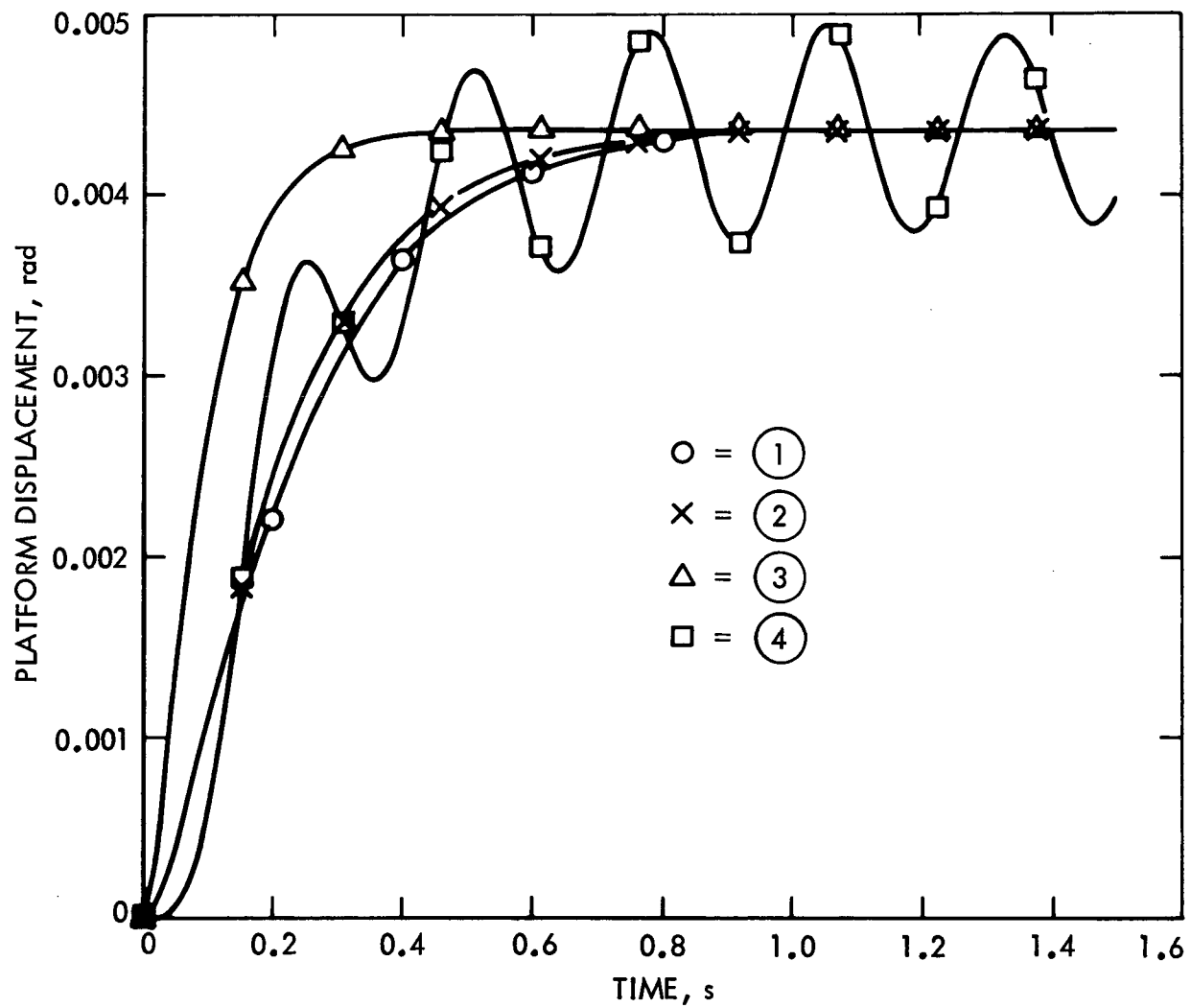


Fig. 7. Scan platform model angular displacements

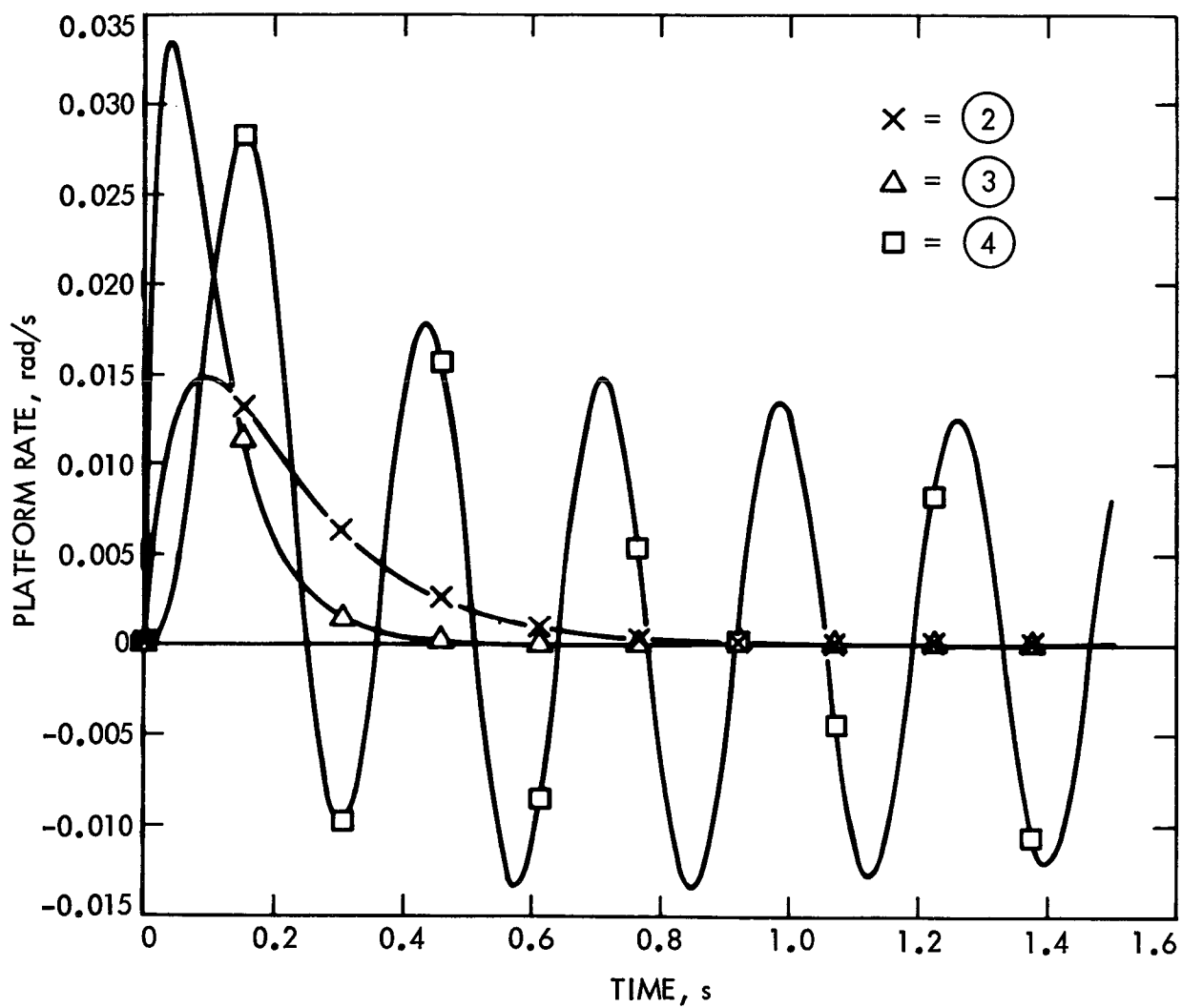


Fig. 8. Scan platform model angular rates

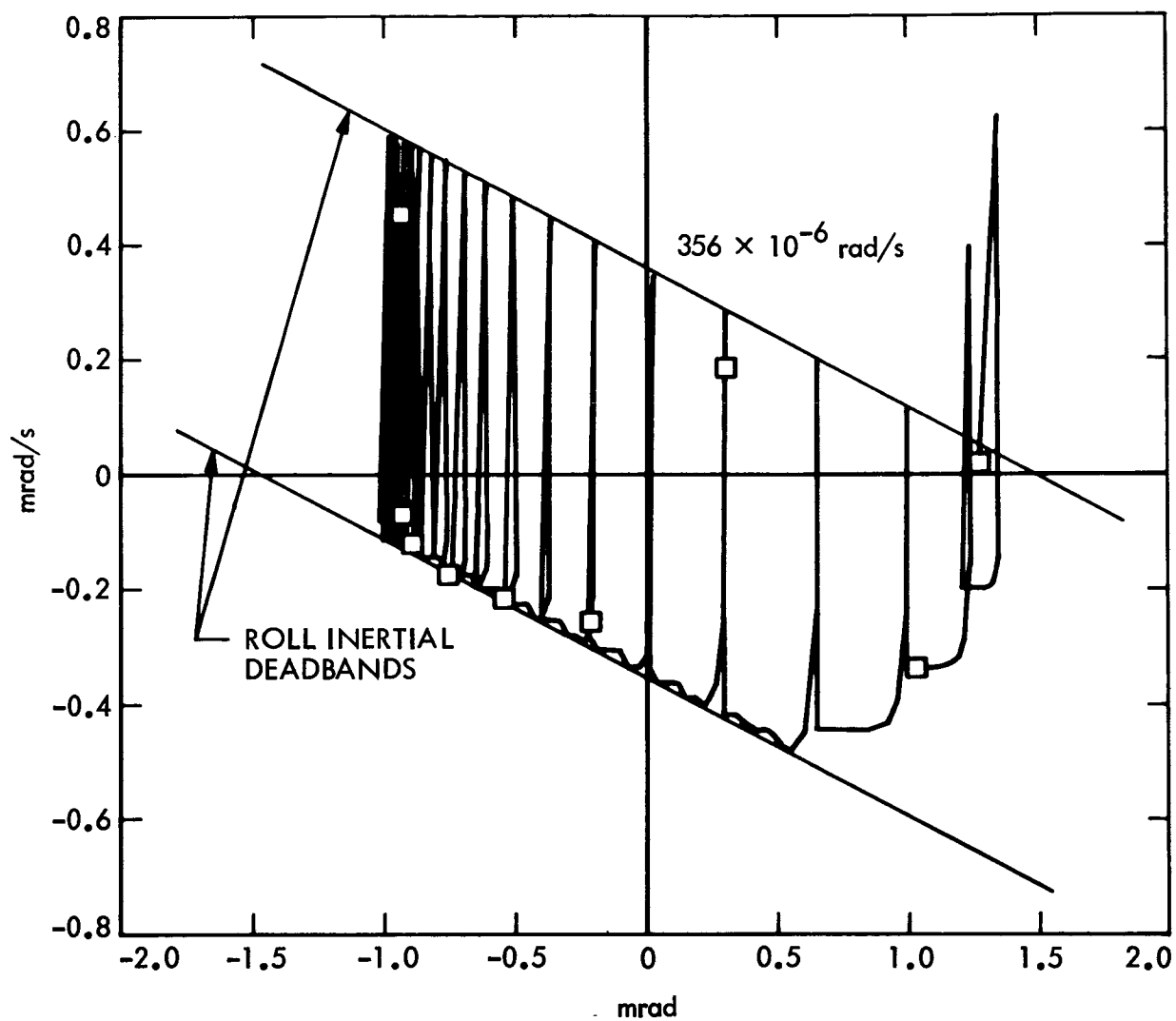


Fig. 9. Roll-axis phase plane during a scan slew; rate disturbance exceeds roll-axis rate plus position deadband

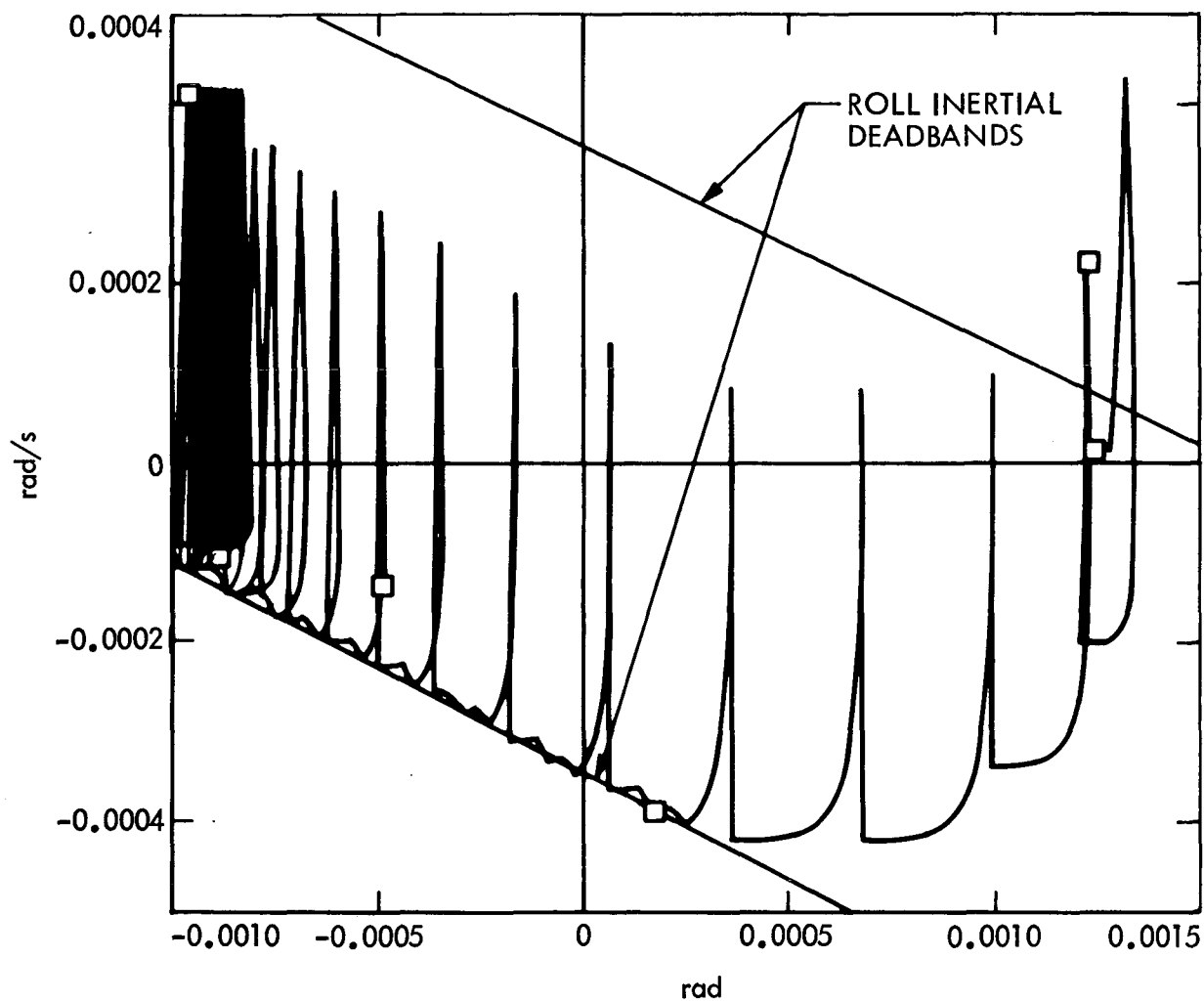


Fig. 10. Roll-axis phase plane during a scan slew;  
roll rate is less than total rate deadband

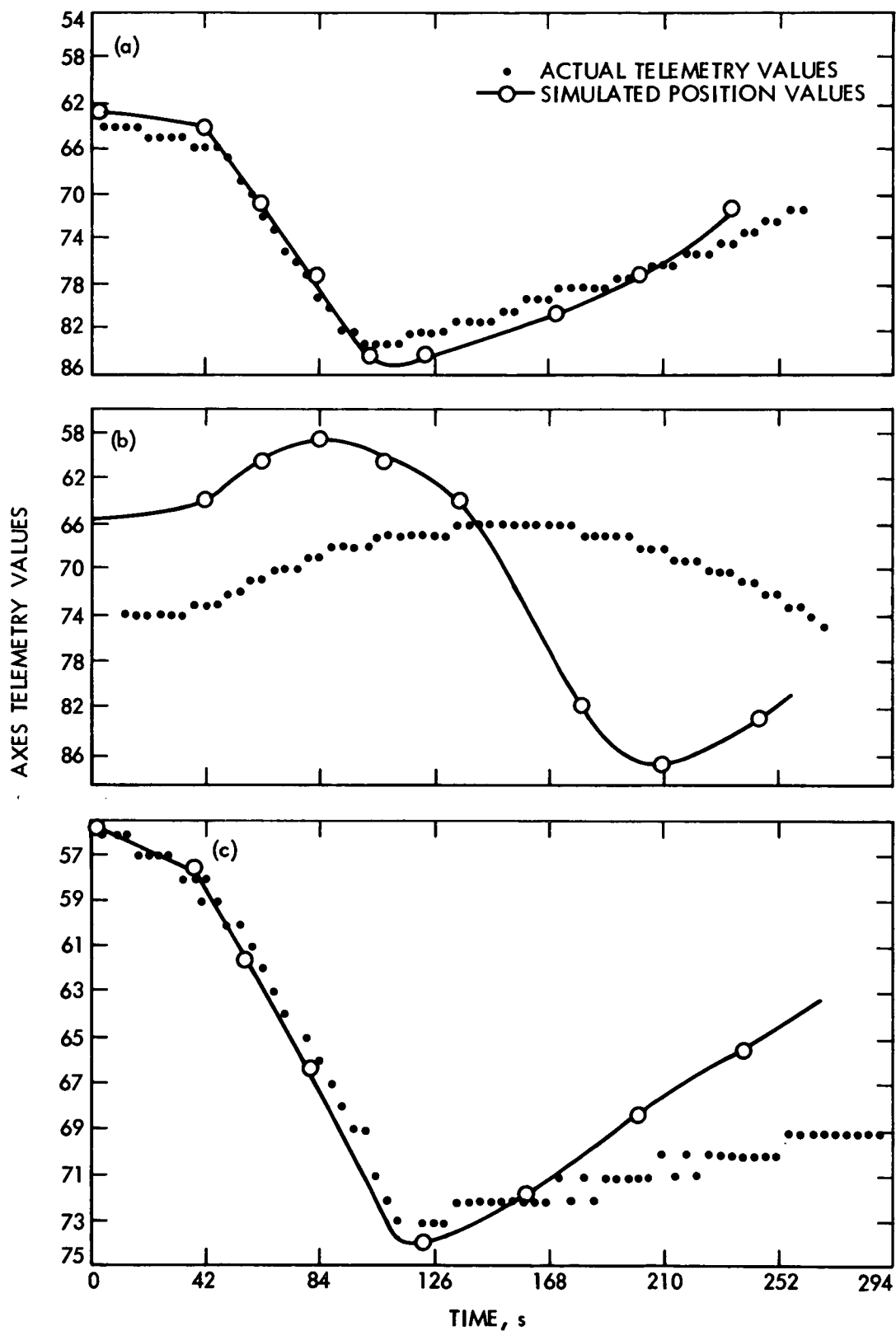


Fig. 11. Comparison of actual and simulated spacecraft position values during a clock-axis slew:  
a. Pitch, b. Yaw, c. Roll

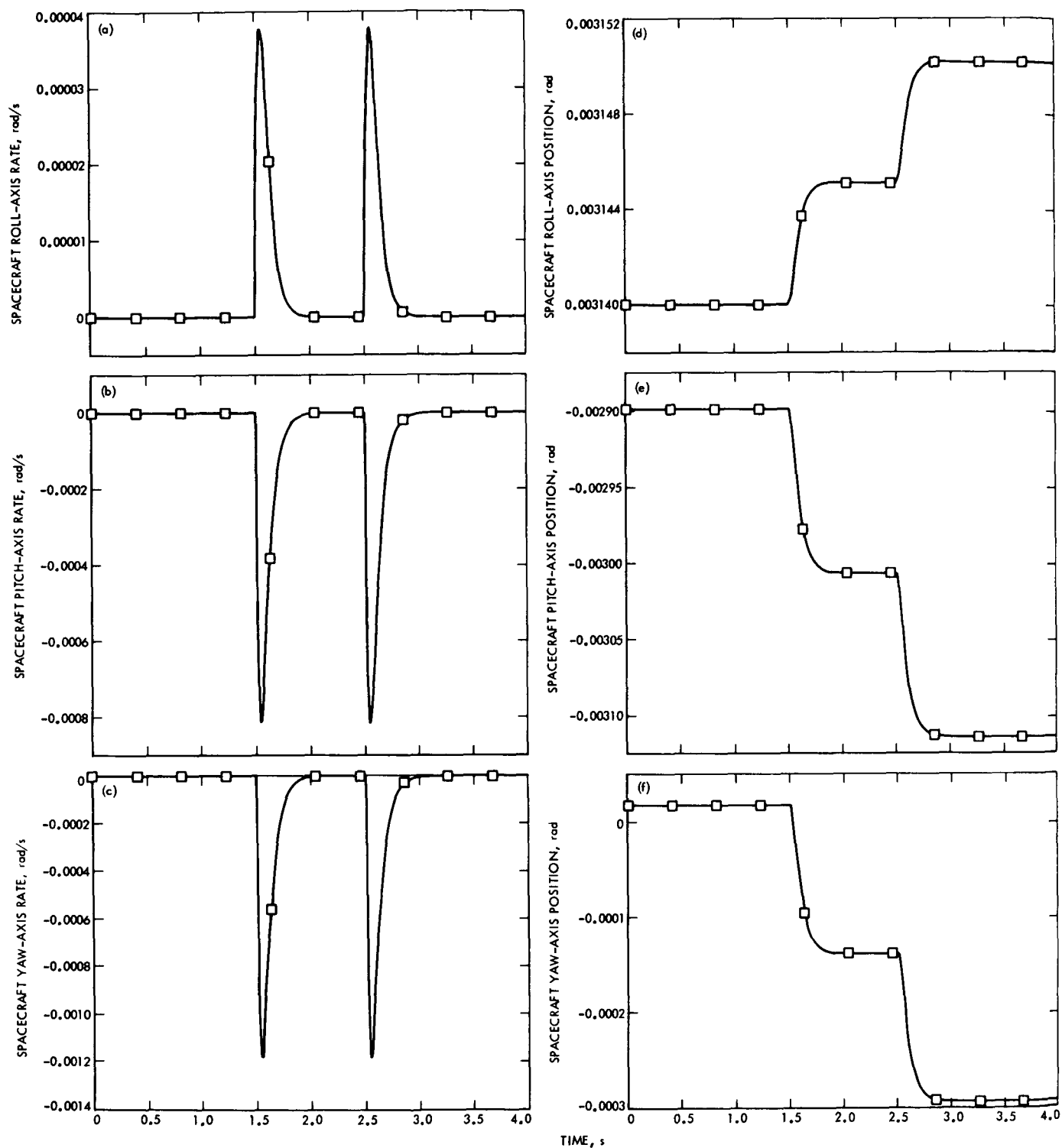
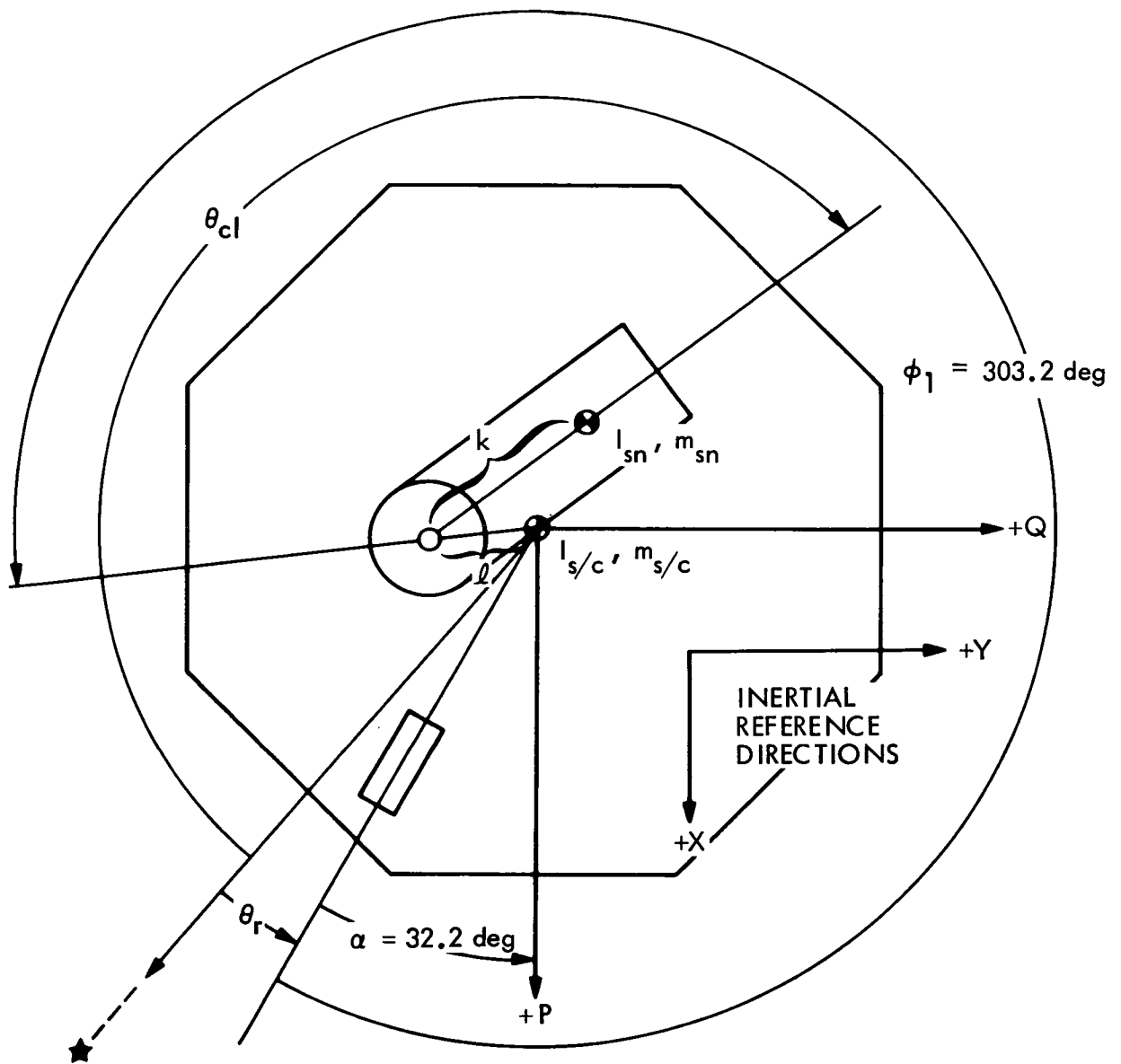


Fig. 12. Spacecraft rate and position during two 0.25-deg cone-axis steps



$$X_{sn} = X_{s/c} + l \cos (\phi_1 - \alpha + \theta_R) + k \cos (\theta_{cl} + \alpha - \theta_R)$$

$$Y_{sn} = Y_{s/c} + l \sin (\phi_1 - \alpha + \theta_R) - k \sin (\theta_{cl} + \alpha - \theta_R)$$

$$\theta_{s/c} = \phi_1 - \alpha + \theta_R$$

$$\theta_{sn} = 2\pi - (\theta_{cl} + \alpha - \theta_R)$$

Fig. 13. MM'71 clock-axis configuration

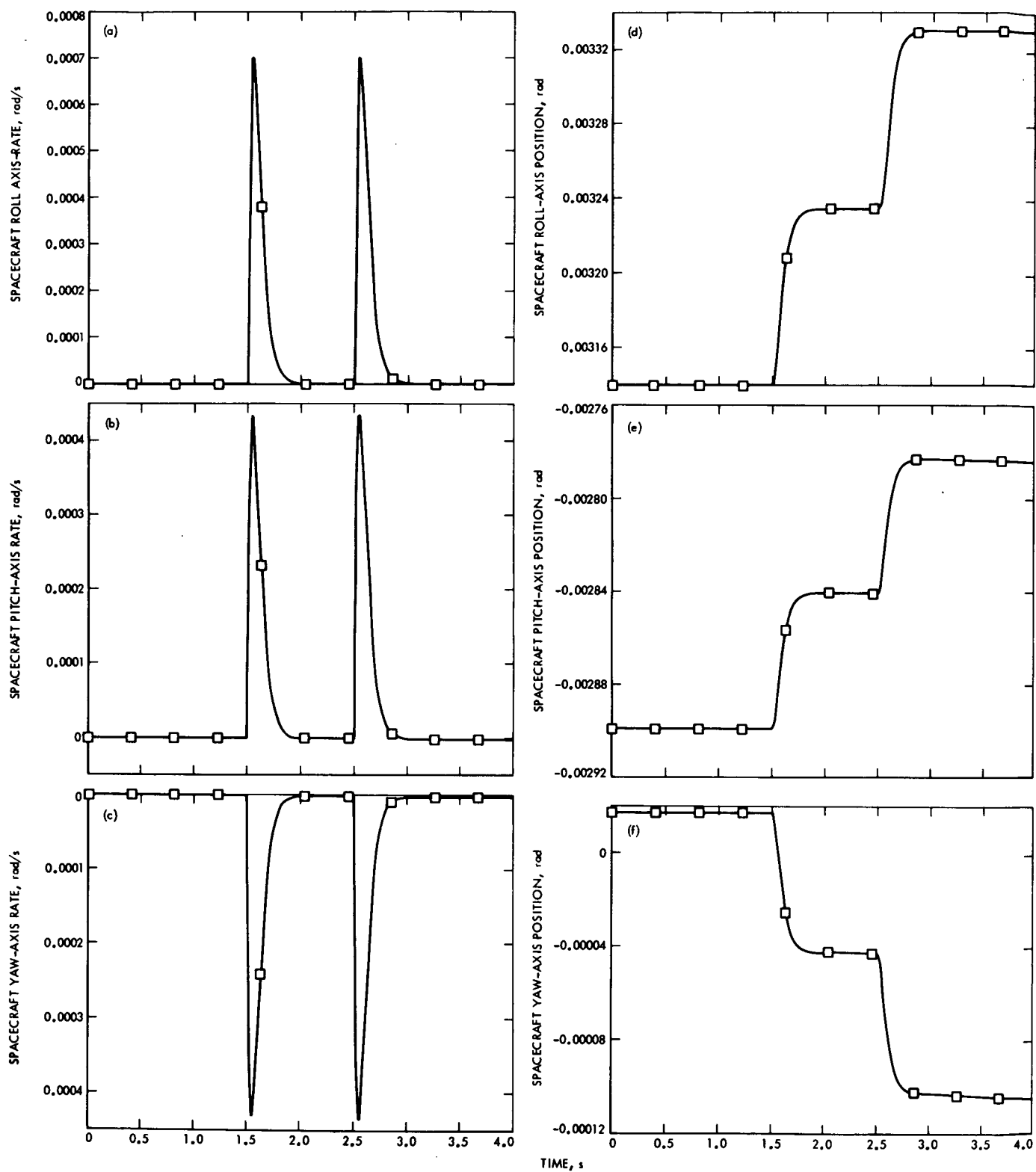


Fig. 14. Spacecraft rate and position during two 0.25-deg clock-axis steps

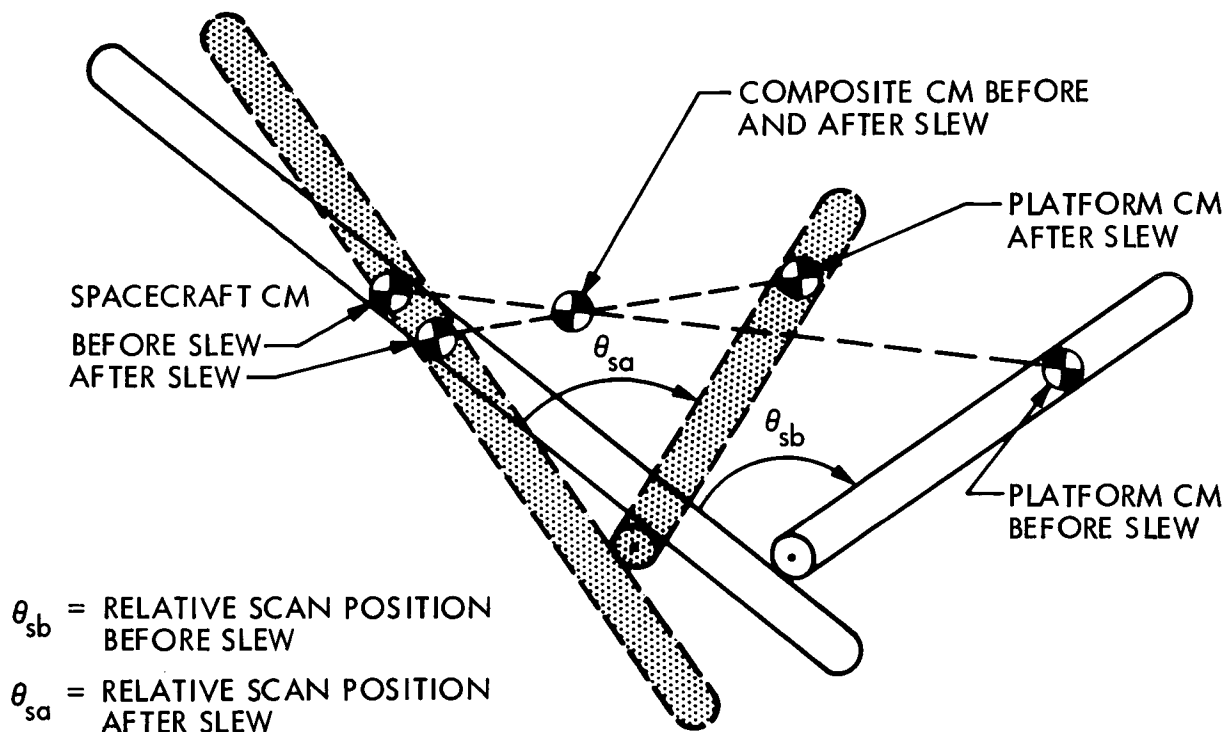
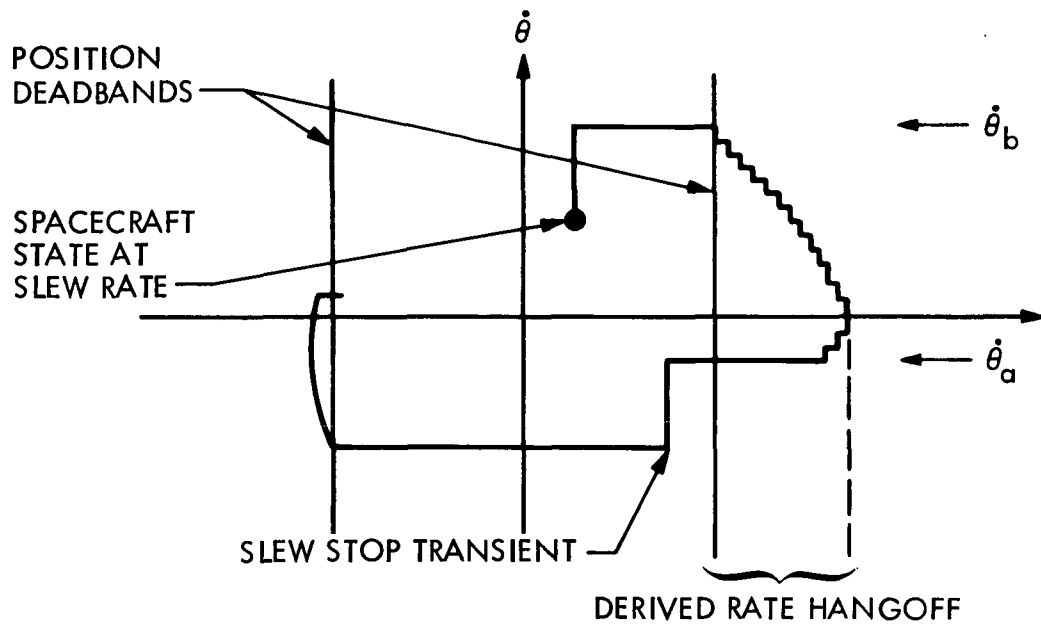


Fig. 15. Center-of-mass relationships before and after a scan slew

(a)



(b)

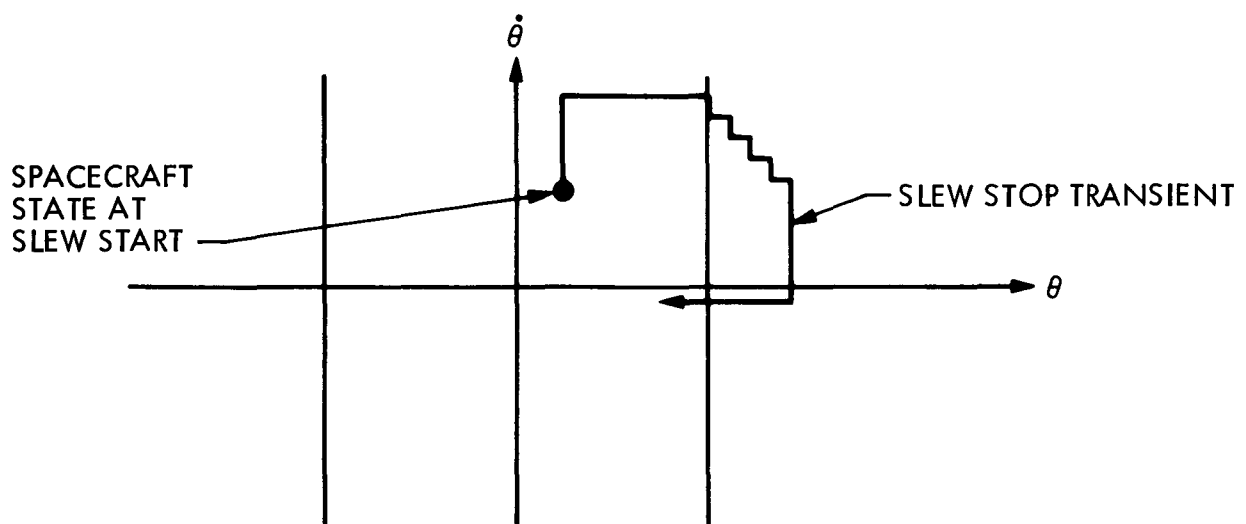


Fig 16. Spacecraft phase plane during (a) long- and (b) short-duration slews

## APPENDIX A. SCAN DESIGN ANALYSIS

The MM'71 scan platform control system design was based on the following linearized analysis and assumptions.

The servo loop torque equations may be expressed as follows:

$$T_m = -K_w \dot{\theta}_m + K_t V - T_l \quad (A-1)$$

where

$$T_m = \text{torque developed by the servo motor} = I_m \ddot{\theta}_m$$

$$I_m = \text{inertia of the motor rotor and gears attached directly to this shaft}$$

$$\approx 9.5 \times 10^{-8} \text{ kg m}^2$$

$$\dot{\theta}_m = \text{motor rotor angular rate}$$

$$\ddot{\theta}_m = \text{motor rotor angular acceleration}$$

$$K_w = \text{motor damping constant} = 2.68 \times 10^{-6} \text{ N-m/rad/s}$$

$$K_t = \text{motor torque constant} = 3.87 \times 10^{-6} \text{ N-m/rad/s}$$

$$V = (\theta_c - \theta_q) G_n \quad (A-2)$$

where

$$V = \text{control winding voltage}$$

$$\theta_c = \text{commanded motor platform position}$$

$$\theta_q = \text{actual platform position}$$

$$G_n = \text{pickoff and amplifier gains to the control winding}$$

$$= 832 \text{ V}_{\text{rms}}/\text{rad}$$

$$N = \text{gear ratio} = 27,000:1$$

$$T_1 = \frac{I_{sn} \ddot{\theta}_q}{RN} \quad (A-3)$$

where

$T_1$  = torque produced at the platform

$I_{sn}$  = scan platform load inertia at the axis of revolution  $\approx 7.87 \text{ kg m}^2$

$\ddot{\theta}_q$  = angular acceleration of the scan platform

$R$  = gear train torque transmission efficiency = 0.4

Assuming that

$$\theta_q = \frac{\theta_m}{N} \quad (A-4)$$

and taking the Laplace transformation of Eqs. (A-1) through (A-4), we obtain the following transfer function:

$$\frac{\theta_q(S)}{\theta_c(S)} = \frac{RNK_t G_n}{(I_{sn} + I_m RN^2)S^2 + K_w RN^2 S + RNK_t G_n}$$

This transfer function is illustrated in block diagram form in Fig. 6a.

## APPENDIX B. SCAN DESIGN ANALYSIS MODIFICATION

This appendix is an extension of the analysis presented in Appendix A. However, in this instance, the displacement of the scan platform ( $\theta_q$ ) is not constrained to be directly proportional to the servo motor displacement. The actuator mechanism linking the servo motor shaft to the platform is modeled as a stiff spring. The torque transmitted from the motor to the platform mass is expressed by

$$T_1 = k_h \left( \frac{\theta_m}{N} - \theta_q \right) \quad (B-1)$$

where  $k_h$  = the stiffness of the actuator mechanism  $\approx 4068$  N-m/rad.

The scan platform displacement is now governed by the equation

$$T_1 = I_{sn} \ddot{\theta}_q \quad (B-2)$$

Taking the Laplace transform of Eqs. (A-1), (B-1), and (B-2), we obtain the following transfer function:

$$\frac{\theta_q(S)}{\theta_c(S)} = \frac{K_t G_n}{\left[ \frac{N I_m I_{sn}}{k_h} S^4 + \frac{N K_w I_{sn}}{k_h} S^3 + \left( N I_m + \frac{I_{sn}}{R N} \right) S^2 + K_w N S + K_t G_m \right]}$$

This transfer function is illustrated in block diagram form in Fig. 6c.

## APPENDIX C. DETERMINATION OF RELATIVE SCAN PLATFORM RATE AND POSITION EXPRESSIONS

The expressions for the rate and displacement of an articulated package relative to the spacecraft bus are derived in this appendix. The inertia of the articulated package is assumed small relative to the spacecraft bus inertia, so that the bus can be assumed fixed during package motion. Figure 5 illustrates the articulated package model for this relative displacement analysis. The command to move the package is assumed to be a stepwise function. For a single step, the Laplace transform of the equation of motion is

$$I_{sn} S^2 \theta_{sn}(S) + f_h S \theta_{sn}(S) + k_h \left[ \theta_{sn}(S) - \theta_{snc}(S) \right] = 0 \quad (C-1)$$

where

$S$  = Laplace operator

$\theta_{sn}(S)$  = Laplace transform of the articulated package displacement

$\theta_{snc}(S)$  = Laplace transform of the commanded package displacement, a step function

$$= \frac{\theta_{snc}}{S}$$

$f_h$  = viscous damping coefficient of the actuating mechanism

$k_h$  = stiffness of the actuating mechanism

Solving Eq. (C-1) for the Laplace transform of the articulated package relative position gives

$$\theta_{sn}(S) = \frac{\theta_{snc} k_h}{I_{sn} S \left( S^2 + \frac{f_h}{I_{sn}} S + \frac{k_h}{I_{sn}} \right)} \quad (C-2)$$

The inverse Laplace transform of Eq. (C-2) for the case of damping greater than critical damping results in the following expressions for the relative displacement of the articulated package:

$$\theta_{sn}(t) = (Ae^{at} + Be^{bt} + K)\theta_{snc} W_n^2 \quad (C-3)$$

where

$$a = (-\alpha + \sqrt{\alpha^2 - 1})W_n$$

$$b = (-\alpha - \sqrt{\alpha^2 - 1})W_n$$

$$\alpha = \frac{f_c}{f_h} = \text{damping ratio}$$

$$f_c = \text{critical damping value} = 2 I_{sn} W_n$$

$$W_n = \text{natural frequency of the actuator-articulation platform system}$$

$$= \sqrt{\frac{K_h}{I_{sn}}}$$

$$A = \frac{1}{a(a - b)}$$

$$B = \frac{1}{b(b - a)}$$

$$K = \frac{1}{ab}$$

The Laplace transform of the spacecraft rate can be obtained from Eq. (C-2) by multiplying by the Laplace operator S, and the inverse Laplace transform results in the following time domain expression for the relative scan rate:

$$\dot{\theta}_{sn}(t) = (Ce^{at} + De^{bt})\theta_{snc} W_n^2 \quad (C-4)$$

where

$$C = \frac{1}{(a - b)}$$

$$D = \frac{1}{(b - a)}$$

Differentiating Eq. (C-4) relative to time and setting the result equal to zero yields the following expression for the maximum spacecraft rate:

$$\dot{\theta}(t)_{\max} = C \left[ \left( \frac{b}{a} \right)^{C_a} - \left( \frac{b}{a} \right)^{C_b} \right] \theta_{\text{snc}} W_n^2$$

## NOMENCLATURE

$F$	reaction force acting at the platform/spacecraft hinge point perpendicular to the slewing axis of revolution
$F_x$	reaction force at the spacecraft bus/scan platform hinge point in the inertial X direction
$F_y$	reaction force at the spacecraft bus/scan platform hinge point in the inertial Y direction
$f_h$	viscous damping in the spacecraft/platform hinge
$I_{pp}, I_{yy}, I_{rr}$	spacecraft bus principal moments of inertia
$I_{s/c}$	moment of inertia of the spacecraft bus about an axis through the center of mass and parallel to the axis of platform revolution
$I_{sn}$	moment of inertia of the scan platform about the center of mass evaluated about an axis parallel to the axis of platform revolution
$I_{sx}, I_{sy}$	spacecraft bus products of inertia measured relative to a coordinate system, two axes of which are perpendicular to the direction of definition for $I_{s/c}$
$k_h$	stiffness of the spacecraft platform hinge
$k$	distance from the scan platform center of mass to the hinge point
$\ell$	distance from the spacecraft bus to the scan hinge point
$m_{s/c}$	mass of the spacecraft bus
$m_{sn}$	mass of the scan platform
$P_h, Y_h, R_h$	scan platform hinge coordinates in the spacecraft P, Y, R coordinate system
$T_h$	spring restraining torque at the scan platform/spacecraft bus hinge point

## NOMENCLATURE (contd)

$T_p, T_y, T_r$	torques about the spacecraft pitch, yaw, and roll axes, respectively.
$X_{s/c}, Y_{s/c}$	inertial coordinates of the spacecraft bus center of mass
$X_{sn}, Y_{sn}$	inertial coordinates of the scan platform center of mass
$\theta_q$	position of the scan platform relative to a reference direction fixed in the spacecraft bus
$\theta_{snc}$	commanded scan platform position
$\theta_{s/c}$	inertial angular displacement of the spacecraft bus
$\theta_{sn}$	inertial angular displacement of the scan platform

## REFERENCES

1. Lin, H. S. , Scan Platform Motion Effects on the MM'71 Attitude Control System, Engineering Memorandum 344-226-HSL, Jet Propulsion Laboratory, Pasadena, Calif. , June 4, 1969 (JPL internal document).
2. Fleischer, G. E. , Multi-Rigid-Body Attitude Dynamics Simulation, Engineering Memorandum 344-275-GEF, Jet Propulsion Laboratory, Pasadena, Calif. , June 19, 1970 (JPL internal document).
3. Kerner, T. , Mariner Mars 1969 Scan Control Subsystem Design and Analysis, Technical Report 32-1506, Jet Propulsion Laboratory, Pasadena, Calif. , October 30, 1970.
4. Edmunds, R. S. , MM'71 Gas Consumption for Scan Slews, Interoffice Memorandum 344-164, Jet Propulsion Laboratory, Pasadena, Calif. , March 14, 1972 (JPL internal document).